LBL-13103

DISCLAIMER

Observation of Anomalous Reaction Mean Free Paths

Of Nuclear Projectile Fragments in Research Emulsion

From 2 A GeV Heavy Ion Collisions

Yasha J. Karant

Nuclear Science Division
Lawrence Berkeley Laboratory
University of California
Berkeley, CA 94720

This work was supported by the Director, Office of Energy Research Division of Nuclear Physics of the Office of High Energy and Nuclear Physics of the U.S. Department of Energy under Contract Number DE-AC03-76SF00098.

CONTENTS

	Page
LIST OF ABBREVIATIONS	iv
I. Introduction and History	1
II. Underlying Physics	3
III. Systematics and Method of Observation	6
IV. Statistical Methods	
A. Method A	12
B. Method B	19
C. Monte Carlo Simultations	28
V. Results	
A. Method A	33
B. Method B	39
VI. Conclusions	43
Acknowledgements	50
References	52
Figure Captions	55
Figures	57

Observation of Anomalous Reaction Mean Free Paths of Nuclear Projectile Fragments in Research Emulsion from 2A GeV Heavy Ion Collisions

Yasha Jack Karant
Ph.D. Thesis

Lawrence Berkeley Laboratory
University of California
Berkeley, California

ABSTRACT

From an analysis of 1460 projectile fragment collisions in nuclear research emulsion exposed to 2.1 A GeV ^{16}O and 1.9 A GeV ^{56}Fe at the Bevalac, evidence is presented for the existence of an anomalously short interaction mean free path of projectile fragments for the first several cm after emission. The result is significant to beyond the 3 standard deviation confidence level.

I. Introduction and History

Sporadic observations in nuclear research emulsion evidencing a short mean free path component among relativistic projectile fragments of high energy heavy ions in the cosmic radiation have been reported since 1954.[I-1] Because of limited statistics, possible systematic uncertainties, and the impossibility of such a component within known nuclear physics, these observations were never widely accepted. The aim of this Bevalac experiment was to obtain sufficient statistics under controlled conditions to obtain an answer to the question (significant at the level of a few percent component): is there evidence for a short mfp (mean free path) component among PFs (projectile fragments) at 2 A GeV?

Fortunately, both the validity of the technique and its results on primary beams are well established. The basic method is the along the track scan. One simply follows each track until it either interacts or exits the detector. An interaction in such a scan is defined to be the emission of at least one hadronic track, either from the projectile or a struck nucleus in the emulsion. Usually, one observes considerably more than one emitted track; because of this, interactions in emulsion are called "stars".

Several preceding experiments had obtained in this fashion the mfps of primary beam nuclei to a statistical precision of 3%. Specific to this result, mfps of ^{4}He, ^{12}C ^{14}N, and ^{16}O had been obtained at LBL[I-2] and ^{16}O at NRC[I-3]. As part of this experiment, primary ^{40}Ar

and ^{56}Fe mfps were measured at LBL and ^{4}He and ^{56}Fe at NRC. In all cases, the measurements were done at about 2 A GeV, although some were also done at other energies to obtain energy dependence information. As will be shown, the 2 A GeV primary beam measurements are in excellent agreement with the measurements on PFs beyond about 5 cm from their emission point. However, below this distance, one observes significant and regular deviations from both the primary beam measurements and the "long distance" observations. Further, the results of the two independent observations, PFs from ^{56}Fe at LBL and ^{16}O at NRC, are in agreement.

In outline, this work will be organized in six parts. This first brief part merely sets the stage for what follows. Part II discusses what one would expect to observe for PFs based on known nuclear physics, while Part III discusses the systematics and techniques actually used in this research. Part IV is a statistical discussion of the formal methods needed to analyze the data in a cogent fashion, and includes a section on Monte Carlo simulations to test the formalism and its physical approximations in light of the material in Parts II and III. Part V is a statement of the results using the methods of Part IV, while Part VI presents the physical conclusions of the investigation.

II. Underlying Physics

To establish that an observation is anomalous, one first needs to know what is normal. In this case, one needs to know the normal interaction behavior of nuclei in emulsion, particularly nuclei of kinetic energy between 1.5 and 2 A GeV. This is given in its simplest form by the total (or inclusive) reaction mfp, normally symbolized by "λ".

One measures mfps, not cross sections, because emulsion is a known mixture of various elements from H to Ag[II-1]. While the measurement techniques and the statistical properties of λ shall be discussed in later sections, the mfp has a simple physical interpretation in terms of number densities and cross sections, namely:

$$\lambda = \left(\sum_{i=1}^{N} n_i \quad \sigma_{OBS}^{i} \right)^{-1} \qquad \text{(II-1)}$$

Here N is the number of different nuclides in the emulsion, n_i is the number/unit volume of nuclide "i", and σ_{OBS}^{i} is the cross section for the projectile to interact in an observable fashion with component "i". σ_{OBS} is defined to include the detection efficiency. Note that λ and σ are inversely related, so that a large σ gives a short λ. It is to be stressed, however, that one measures λ, not σ_i; nonetheless, a knowledge of the properties of λ carries over to information about σ.

To an excellent approximation, the σ_{OBS}'s in question are just a constant fraction of the reaction cross section. Two properties of heavy ion reaction cross sections are of importance to this work: from about 0.5 A GeV to > 2 A GeV i) σ_{OBS} are essentially constant and ii) they are well described by a geometrical dependence.[II-2]

In its simplest approximation, the reaction cross section is expressed in the Bradt-Peters form,[II-3]

$$\sigma_{12} = \pi r_0^2 \, (A_1^{1/3} + A_2^{1/3} - n)^2 \qquad \text{(II-2)}$$

where r_0 and n are constants and A_1, A_2 are the baryon numbers of target and projectile. If $A_1^{1/3} >> A_2^{1/3} - n$

$$\sigma \propto A^{2/3}$$

Since $A \propto Z$ near the valley of stability (VOS), one might guess that

$$\sigma \propto Z^{2/3}$$

This suggests as a first approach, a behavior of the form

$$\lambda = \Lambda Z^{-b} \qquad \text{(II-3)}$$

with $b \approx 2/3$. In fact, this does adequately fit the primary beam data, with $b \approx 0.4$.

The equations to be solved for estimating Λ and b are presented in Section IV. Using these, one obtains two fits; one for LBL, the other for NRC.

At NRC: $\Lambda^* = 28.9 \quad 2.5$ cm, $b^* = 0.43 \pm 0.04$

At LBL: $\Lambda^* = 32.2 \quad 2.5$ cm, $b^* = 0.44 \pm 0.03$

While the consistency of the observations is evident, one must realize that these are measurements of nuclides limited to the VOS.

Classical nuclear physics predicts that not only VOS nuclides are present in PFs but also isotopes away from the VOS as well as various excited states with lifetimes $c\tau \geq 1$ cm. To incorporate the deviations these effects might produce in the mfps (which are really a function of Z, A and quantum state) one has two alternatives.

The obvious, empirical method would be to measure all these mfps. It is equally obvious that the logistics of such a measurement would be intractable. An alternative, albeit somewhat less secure, option is to obtain calculated values based on realistic models that use other experimental data, such as form factors and detection efficiency[II-4]. This is what was done. The results are displayed in fig. II-1, along with the fits to data and observations. While the general trend is reproduced, there does appear to be a theoretical prediction that the Z = 3,4,5 isotopes will fall below the fitted lines. Additionally, isotopic "noise" is visible. In section VI-C, dealing with the Monte Carlo simulation, the methodology for dealing with this will be discussed.

III. Systematics and Method of Observation

In this section, three main points are discussed: the quantities which were measured, how the measurements were actually conducted, and the systematic problems posed by these measurements. This begins with a consideration of the method of scanning actually adopted.

At both NRC and LBL, an unbiased forward along the track scan was used. This means that a primary track was picked up on the scan line as it entered the stack; the scan line was typically 2 mm from and parallel to the leading milled edge of each pellicle. The track was examined to insure that it did not interact before the scan line. At LBL, primaries were followed until they either interacted or left the pellicle; at NRC, primaries were followed until they interacted or left the stack. When the primary interacts, any PF produced is classified as a secondary. When a secondary PF interacts, any PF produced is a tertiary, and so on. All PFs of $Z \geq 3$, regardless of generation (secondary, tertiary,...), were followed until they interacted or left the stack.

Both stacks were Ilford G-5 emulsion, made up of pellicles nominally 600 μm thick at exposure. The NRC stack had 50 pellicles 15 x 30 cm^2; the LBL stack had 42 pellicles, 7.5 x 12 cm^2. The stacks were processed separately at LBL but using basically the same procedure. A 1 mm^2 grid was photographed on each pellicle before being removed from its respective stack, mounted on glass and processed.

Projectile fragments are nuclei produced by a relativistic heavy ion collision essentially at the velocity of the projectile. Spectrometer studies have shown that the average momentum shift in the laboratory frame of a PF relative to its parent is on the order of -150 MeV/c at ≈ 3 A GeV/c nucleon[III-1]; hence, the major cause of energy loss is ionization. This point shall be examined in the discussion of the energy spectra of the PFs. At the energies used in this work, PFs of $Z \geq 3$ are confined to a narrow forward cone.[III-2] PFs were only accepted within the forward 6° cone; in the processed pellicles, one must correct for the shrinkage factor in the pellicle thickness between exposure and scanning.

One must also be able to measure charge since the mfp is a function of baryon number A and hence Z. At the time of detection of each PF track, its charge was visually estimated as light, medium, or heavy, but actual charge determination was done as a separate step of the measurement after the topology of the event was completed. This assured a second observation of the vertex.

To determine the reproducibility of the charge measurements, the method of repeated observations was used at LBL. By this method, a track was chosen at random which had been first measured to give charge Z_1, say. Subsequent independent observations were made on different segments of the same track, yielding measurements $Z_2 \ldots Z_N$. The deviations Z_1-Z_2, $Z_1-Z_3, \ldots Z_1-Z_N$ were histogrammed, and since for the different Z_1s the results of Z_1-Z_i were compatible, one final histogram was produced (fig. III-1a). This yielded an empirical

charge reproducibility of 1 charge from $6 \leq Z \leq 26$. These deviations were obtained at different depths and plates to verify the correction for development gradients and test the hypothesis of plate-to-plate uniformity. Further, they were examined for a systematic shift with distance into the stack; such a shift could indicate a change in track structure due to a slowing fragment. No such shifts were found, lending further credence to the assumption that one was in fact dealing with relativistic PFs.

The procedure used at NRC was comparable, except that a higher statistical accuracy was obtained, in part because of the smaller charge range here reported ($3 \leq Z \leq 8$). As can be seen from fig. III-1b, charges were measured to a statistical accuracy of 1/3 charge beyond charge 5 and about 1/4 charge for Z = 3 and 4.

An important question is whether or not a systematic error in the charge measurements would have affected the interpretation of the results. Obviously, this would make the absolute determination of the mfp of PFs of charge Z to be in error. However, if one makes comparisons internal to the same observations, this systematic effect is mitigated. In fact, this procedure was tested by several methods. First, by direct observation, the charge measurements do not depend on distance from the emission point of a PF. Second, one may assume a systematic shift of 1, 2 and 3 charge units and compare the relative internal results; while this does affect the absolute mfp value at a given charge, it indeed has no significant effect on the relative answers. Observations that were 3 standard deviations apart remained so.

Since there was no magnetic field of sufficient intensity to obtain meaningful rigidity measurements with the detectors used, no direct measurements of momentum were possible. While multiple scattering would be the only technique available here to directly measure energy,[III-3] it is not nearly sensitive enough under the conditions of this investigation to provide proof that one is dealing with relativistic PFs[III-4]. Nonetheless, some multiple scattering measurements were done at NRC and were entirely consistent with the calculated energy spectra.

To calculate the energy spectra, several pieces of information were utilized. First, the spectrometer measurements on momentum distributions of PFs were used.[III-5] Here, a $p_{\parallel}$ shift of about -150 MeV/c total momentum was observed in the laboratory frame, with an RMS width of about 450 MeV/c to the $p_{\parallel}$ distribution. Consider a mass 10 PF with a parent nucleus of 2.5 A GeV/c or total momentum of 25 GeV/c assuming the persistence of velocity. At the -3 RMS deviation level, it would be shifted downward by -1.5 GeV/c or about 6% of its total momentum. In terms of kinetic energy, this is about an 8% degradation. Hence, one can conclude that even in a worse case analysis (-3 RMS deviations), the effect of kinetic energy/nucleon loss at emission of a PF relative to its parent is small compared to the rather larger losses caused by ionization in the emulsion. Assuming the values given in the literature for the specific ionization constant,[III-6] energy spectra for the PFs in the experiment were calculated, displayed in fig. III-2ab. As can be seen, none of the PFs would have had an energy below 1 A GeV and few below 1.5 A GeV.

I shall conclude this section with a discussion of the scanning itself. As mentioned above, an unbiased forward scan was used in both laboratories. An interaction was defined as the emission of at least one charged hadronic track at the vertex. Distances were measured by projected range in 1/10 of a grid coordinate (100 μm) at LBL and by stage coordinate at NRC. At LBL, the grid coordinates were checked against direct stage measurements.

All data at LBL were rescanned by a different observer using a somewhat different technique from the initial scan. Since one could imagine the potential pitfall of differential scanning efficiency (a scanner being more observant immediately following a vertex), the scanners backscanned all noninteracting PFs and proceeded backward from all observed interaction vertices. About 3 more stars were obtained in this fashion, but the distribution of these stars was the same as the rest, not being confined to long distances (which would have had to be the case if the cause of the anomalous results was a distance dependent scanning efficiency). Scanner-to-scanner comparisons likewise yielded consistent results. In keeping with the fact that two separate experiments are involved, no systematic rescan was done between NRC and LBL; however, several interesting events were cross examined without any difficulty being found.

To diminish scanning loss at NRC, the method of multiple charge measurement was used. Charges were periodically measured along the track; whenever a charge change was indicated, the preceding section of track was examined for a candidate vertex. This naturally increased

the detection efficiency for certain classes of stars at NRC relative to LBL, namely stars with a small charge change to the next generation PF. In both experiments, the scanning was done under $\approx$ 500X magnification, with questionable vertices examined under higher power. In this fashion, spatial resolution to ≤ 1 μm is obtainable.

I defer discussion of certain potential vertex misidentification and background problems to Section VI.

IV: Statistical Methods

A. Method A

The most basic concept of this experiment is the mean free path; hence, one needs a means to estimate this quantity. Assuming a mixture which has a length scale of inhomogeneity small compared to the distance scale of the interaction, the mean free path appears as the parameter λ in the differential equation

$$\frac{dN}{dx} = \frac{-N}{\lambda} \quad . \tag{IV-1}$$

Here, one has a number N of particles incident on a slab of thickness dx and some physical process, characterised by λ, which removes flux. The solution to this equation is well known to be the negative exponential; specifically, the probability density is given by

$$f(x)dx = e^{-x/\lambda} \frac{dx}{\lambda} \tag{IV-2}$$

This form of probability density leads to several consequences. Foremost is the property that the negative exponential "has no memory". Physically, this means that any infinitesimal slab dx is equivalent to any other in which the particle may suffer an interaction, irrespective of the location of the slab. The fact that a particle has not interacted up to dx has no influence on its fate in dx.

Given any sample of tracks in a finite length detector, one may consider two classes of tracks: i) those that did interact and ii) those that did not. Further, one may ask whether to use information regarding only the total numbers that did (and did not) interact or also the distribution of interaction distances. The first method of estimation, which shall be denoted as Method A, uses both a moment of the interaction distance distribution as well as information about those tracks that did not interact. The idealized method is this:

1) Assume λ is a constant.

2) Follow tracks until N interactions are obtained, $N \geq 1$.

3) Sum up the total path length followed of both the interacting and noninteracting tracks, where the path length of a track of an interacting particle is the length from its initial observation until its interaction point. Call this sum S_N.

4) Define the estimate of the mfp $\lambda^* = S_N/N$.

One needs the distribution of λ^* given N and λ; since (N,λ) are fixed, this amounts to the distribution of S_N. The simplest case is that of an infinite detector. Here one wants

$$f(S_N) = \int \theta(x_1) \ldots \int \theta(x_n) \quad \theta(S_N) \quad \delta(S_N - \sum_{i=1}^{N} x_i) \prod_{i=1}^{N} \frac{dx_i}{\lambda} e^{-X_i/\lambda} \tag{IV-3}$$

Note that this has dimensions $(\text{length})^{-1}$, which is correct, since the differential dS_N has dimensions length. The above is the convolution of the densities. To obtain insight into the above integral, consider the case N = 2. One wants

$$\int_0^{S_2} e^{-x/\lambda}\, e^{-(S_2-x)/\lambda}\, \frac{d\cdot}{\lambda^2} = \frac{S_2}{\lambda}\, e^{-S_2/\lambda} \qquad \text{(IV-4)}$$

By construction,

$$\int_0^{\alpha} dS_2\, \frac{S_2}{\lambda^2}\, e^{-S_2/\lambda} = 1$$

so I assert that the probability for observing $S_2 \leq X$ is

$$P(0 < S_2 \leq X) = \int_0^X dS_2\, \frac{S_2}{\lambda^2}\, e^{-S_2/\lambda} \qquad \text{(IV-5)}$$

An examination of classical distributions reveals a great similarity of eqn. IV-5 to the χ^2 distribution

$$P(\chi^2/\nu) = \frac{1}{2^{\nu/2}\Gamma\left(\frac{\nu}{2}\right)} \int_0^{\chi^2} dt\, t^{\nu/2-1}\, e^{-t/2} \qquad \text{(IX-6)}$$

Let $\nu = 4 \Rightarrow$

$$P = \frac{1}{2^2\Gamma(2)} \int_0^{\chi^2} dt\, t\, e^{-t/2}$$

Now let

$$S_2/\lambda = t/2 \Rightarrow t = \frac{2S_2}{\lambda}\ , \quad dt = \frac{2}{\lambda}\, dS_2$$

So

$$P = \frac{1}{4} \int_0^{\chi} \frac{2dS_2}{\lambda}\, \frac{2S_2}{\lambda}\, e^{-S_2/\lambda}$$

$$= \int_0^{\chi} S_2\, e^{-S_2/\lambda}\, \frac{dS_2}{\lambda^2}$$

Hence, one may profitably conjecture that $2S_N/\lambda$ is distributed like χ^2, with $\nu = 2N$ DOF. In fact, it is rather simple to see that

this must be the case. It is clear by inspection that a single exponential deviate from a distribution with parameter λ (i. e., S_1) is isomorphic with a variable $2\ S_1/\lambda$ which is distributed like χ^2 with 2 DOF. Further, it is an elementary property of the χ^2 family that the sum of any set of χ^2 deviates is itself a χ^2 deviate with DOF equal to the sum of the DOF of each member of the set. By combining the isomorphism of the distribution of S_1 with the χ^2 distribution, and using the above mentioned property of the χ^2 distribution, the result immediately follows.

Having established the distribution of S_N in an infinite detector, one can now apply it to the case of a finite detector. As long as there is an essentially unlimited number of tracks so that in any repeat experiment one can go to the Nth interaction, then the distribution must be the same. To establish this fact physically, I invoke the no-memory property. Simply regard each track length in an infinite detector as made up of noninteracting segments plus the last segment, which terminates in an interaction. In an infinite detector, each track must interact, causing N to be identical to the number of tracks; in a finite detector, N is related to the fluence Φ by the binomial distribution at fixed fluence, so that one in principle requires an arbitrary number of particles to ensure absolutely in all cases that one reaches N. In fact, let T be the distance available for observation and $P_T = 1 - e^{-T/\lambda}$; then N is distributed

$$\binom{\Phi}{N} p_T^N (1 - p_T)^{(\Phi - N)}$$

As a practical matter, I consider the distribution of $2S_N/\lambda$ to be χ^2 with 2N DOF; one thereby has for use the whole classical armory of the χ^2 family. In particular, suppose one has measured λ_1^*, with N_1 interactions and λ_2^* with N_2 interactions, both from a population with supposedly the same λ.

Let $f_{12} \equiv \lambda_1^*/\lambda_2^*$. One sees that f_{12} is distributed like the F variance ratio with $2N_1$ and $2N_2$ DOFs. Classically,

$$F = \left(\chi_1^2/\nu_1\right)\Big/\left(\chi_2^2/\nu_2\right) = \left(\frac{2S_{N_1}}{\lambda}\Big/2N_1\right)\Big/\left(\frac{2S_{N_2}}{\lambda}\Big/2N_2\right) \tag{IV-7}$$

$$= \left(\frac{S_{N_1}}{N_1}\right)\Big/\left(\frac{S_{N_2}}{N_2}\right) = \lambda_1^*/\lambda_2^* = F_{12}$$

Most important, <u>this ratio F is independent of any assumed value of λ</u>.

One of the great values of using classical distributions is that their cumulative distribution functions (CDF) are well known and hence available in standard computational tables and algorithms. The CDF is normally associated with a probability for a continuous random variable; if one uses the one-sided integral from the lower limit of the possible values of the variable to the observed value and the observations obey the physics used to derive the CDF, then one has the very important result, namely:

The distribution of probability values is uniform from 0 → 1.

In particular, the uniform distribution U(0,1) has mean = 1/2 and RMS deviation = $1/\sqrt{12}$. If one has N measurements from a distribution assumed to be U(0,1), one can construct the sample mean m. A basic test is to calculate the quantity

$$\sigma = (m - 1/2) \,|\, \sqrt{12N} \tag{IV-8}$$

if $N \geq 5$, σ is essentially a gaussian deviate of mean 0 and variance 1, and tests if the sample mean significantly differs from its expectation value of 1/2.

One specific application of the χ^2 distribution is the use of the method of maximum likelihood to estimate values of (Λ, b) in $\lambda = \Lambda Z^{-b}$ from a set of $\lambda^*(Z)$ measurements, say with N_Z stars each. First, take the logarithm of the probability density of the χ^2 distribution [eqn. IV-6],

$$\ln f = \ln 1/2 - \ln \Gamma(N) + (N - 1) \ln N\lambda^*$$

$$- N \ln \Lambda + N b \ln Z - \frac{N\lambda^* Z^b}{\Lambda}$$

Taking derivatives with respect to Λ and b and letting $S_Z = \lambda^*(Z)N_Z$, one obtains Λ^*, b^* as solutions of

$$\frac{\sum_Z S_Z Z^{b^*}}{\sum_Z N_Z} = \frac{\sum_Z S_Z Z^{b^*} \ln Z}{\sum_Z N_Z \ln Z} \tag{IV-9a}$$

$$\Lambda^* = \frac{\sum_Z S_Z Z^{b^*}}{\sum_Z N_Z} \tag{IX-9b}$$

Having established that the estimate $\lambda^* = S_N/N$ depends essentially only on the true mfp λ and N and is independent of detector size, one can subdivide a data sample and consider $\lambda^*(\eta)$ with η some variable of which λ has a known theoretical distribution. Likewise, one

may construct $\Lambda^*(\eta)$. In particular, η may profitably be taken to be the distance after the point of first observation of a track; call this distance "D_F". In this case it is clear that a constant λ (or Λ) is independent of D_F, and hence λ^* should also be independent of D_F. One may thus consider λ^* binned in distance intervals $D \equiv D_1 \leq D_F \leq D_2$, which should give a consistent result for λ^* irrespective of D_1 or D_2. This method of examining $\lambda^*(D)$, and especially $\Lambda^*(D)$(for a fixed value of b), will be termed method A'.

To conclude this section, a second, and more conventional, application of the χ^2 distribution is noted. The use of χ^2 as the parent distribution of $2S_N/\lambda$ at fixed 2N stars has already been mentioned. This use is <u>not</u> in the standard method of a goodness-of-fit test. However, given a series of observations of S_N and N and an assumed value of λ, one can construct a test of goodness of fit via χ^2 in its more typical application. For clarity, term this Θ^2.

Under the null hypothesis that λ is correct, the integral probability $P(\chi^2, 2N)$ is distributed U(0,1). Hence, to every P_i ("i" denoting the observation number) one may uniquely assign a σ_i, where σ_i is distributed normally with mean 0 and variance 1. This is done by finding that σ_i such that $P(\sigma_i) = P_i$, where $P(\sigma_i)$ is calculated from the gaussian (e.g., $P_i = 0.84134 \Leftrightarrow \sigma_i = 1.00$; $P_i = 0.15866 \Leftrightarrow \sigma_i = -1.00$, etc.). Now $\Theta^2 = \Sigma\sigma_i^2$, and if the null hypothesis is correct Θ^2 obeys a χ^2 distribution. The DOF are also directly obtained: if λ is given independent of the observations in question, DOF = number of observations; if λ is extracted from the observations, DOF = number of observations - 1.

B. Method B

Thus far the statistical analysis has been limited to methods that include both interacting and noninteracting tracks. It is also necessary to consider other forms of analysis, both for the additional insight they give into the nature of this effect and because certain types of information are simply not available in any other way. For example, if one wishes to compare some statistic on distributions of tracks with some characteristic (say those that terminate in stars of multiplicity >N versus those $\leq$N), one of necessity must deal with samples of only those particles which interacted.

For simplicity, convenience, and conformity with physics conventions, I shall demand that any statistic claimed to be a continuous "probability" is distributed U(0,1) if the hypothesis under which it is calculated is true. While this requirement may seem pedantic or obvious, many applications in the field of PF mfp's have subtly ignored this. The problem arises as follows. Suppose one has two manifestly independent events, say, 1 and 2, and under the hypothesis H, one has probability P_1, the other P_2, where P_i is distributed U(0,1). Naively, one says that the probability of 1 and 2 is $P_{12} = P_1 \cdot P_2$. The difficulty is that while P_{12} does go from 0 to 1, it is <u>not</u> a priori uniformly distributed under H; there is nothing special about $\{P_1, P_2\}$ and all products of probabilities that give P_{12} are acceptable. In this case, where events 1 and 2 are truly independent, there is a simple procedure to return to the uniform distribution U(0,1). Let P_1, P_2, ... P_N be the N independent probabilities, each U(0,1). Then

$$h^2 = -2 \sum_{i=1}^{N} \ln P_i \qquad \text{(IV-10)}$$

is distributed like χ^2 with 2N DOF. One now constructs $P(h^2 < \chi^2, 2N)$ and this P is distributed U(0,1) if H is true.

To see that this must be the case, one uses the formalism of method A. For each value of the probabilites assumed U(0,1), p_i say, consider $x_i = -\ln p_i$. Each of these x_i must be an exponential deviate from a distribution with parameter $\lambda = 1$. It has already been established that

$$\frac{2}{\lambda} \sum_{i=1}^{N} X_i$$

is distributed like χ^2 with 2N DOF. Of course,

$$\sum_{i=1}^{N} X_i = -\sum_{i=1}^{N} \ln P_i = -\ln \prod_{i=1}^{N} P_i$$

Begin with the simplest case: the observation of a single interacting track. Under the null hypothesis, there is a known single mfp λ. One measures two quantities: the length to the interaction, X, and the potential path, T, which is the maximum length the individual track could have been observed within the stack (which may change with each individual track). Start with the differential equation

$$\frac{dN}{dx} = -\frac{N}{\lambda}$$

which has solution

$$N = N_o \int_0^X \frac{dx}{\lambda} e^{-x/\lambda}$$

or

$$P(X) = 1 - e^{-X/\lambda} \equiv P_1(X|\lambda) \qquad \text{(IV-11)}$$

However, the maximum P observable is

$$P(T) = 1 - e^{-T/\lambda} = P_1(T|\lambda)$$

hence,

$$P(X|T) = P_1(X|\lambda)/P_1(T|\lambda) \equiv P_1(X|T,\lambda) \qquad \text{(IV-12)}$$

Thus, the use of a finite detector necessitates the renormalization of P(X) by the well-known factor P(T). From this one can construct the probability density

$$f(x|T,\lambda)\, dx = \frac{e^{-x/\lambda}\, dx}{\lambda\left(1-e^{-T/\lambda}\right)} \qquad \text{(IV-13)}$$

and thus the logarithmic likelihood function

$$\ln L(x|T,\lambda) = \frac{-x}{\lambda} - \ln \lambda - \ln\left(1 - e^{-T/\lambda}\right) \qquad \text{(IV-14)}$$

Given an individual (X,T), λ^* is the solution of

$$X = \lambda^* + \frac{T}{1-e^{-T/\lambda^*}} .$$

In general, one plots $\ln L$ versus either λ_Z or $\lambda = \lambda_Z Z^b$.

All of the above results shall be called the one-chain formula. This is so named because it addresses only one track at a time.

However, the single track is not the only topology with which one must deal. Another common topology is the N-chain. The N-chain is the topology when one has N - (one chain)s in a row. Consider the case that will be of particular use here, the two-chain topology. Let X be the interaction length of the first link with mfp λ_x, Y the length of the second link with mfp λ_y, and T the potential path from the start of the first link. The relevant differential equations are

$$\frac{dN_1}{dx} = \frac{-N_1}{\lambda_x} \tag{IV-15a}$$

$$\frac{dN_2}{dx} = \frac{-N_2}{\lambda_y} + \frac{N_1}{\lambda_x} \tag{IV-15b}$$

where the last equation simply means that the loss in N_1 is the increase in N_2.

There are several different probability distributions one may construct from X and Y given the mfps and T. One is P(X), another P(Y), which uses the X and Y information from each two-chain event separately. On the other hand, one may combine all the information into one variable, $S = X + Y$, and consider $P(S|T,\lambda_x,\lambda_y)$ and the likelihood from this. Since the charges Z_x, Z_y are what one actually measures, and one then assumes $\lambda = AZ_x^{-b}$, $\lambda_y = AZ^{-b}$, one may write $P_2(S|T,Z_x, Z_y, A,b)$ and examine the likelihood as a function of one parameter, A, say.

There are two cases to consider i) $\lambda_x \neq \lambda_y$ and ii) $\lambda_x = \lambda_y = \lambda$. To derive the S distributions, elementary integration yields:

$$\text{i)} \quad P_2(\Sigma|\lambda_x,\lambda_y) = 1 - \frac{1}{\lambda_x-\lambda_y}\left(\lambda_x\, e^{-\Sigma/\lambda_x} - \lambda_y\, e^{-\Sigma/\lambda_y}\right) \qquad \text{(IV-16a)}$$

$$\text{ii)} \quad P_2(\Sigma|\lambda) = 1 - \frac{\Sigma}{\lambda}\, e^{-\Sigma/\lambda} - e^{-\Sigma/\lambda} \qquad \text{(IV-16b)}$$

so

$$\text{i)} \quad P_2(S|T,\lambda_x,\lambda_y) = P_2(S|\lambda_x,\lambda_y)/P_2(T|\lambda_x,\lambda_y) \qquad \text{(IV-17a)}$$

$$\text{ii)} \quad P_2(S|T,\lambda) = P_2(S|\lambda)/P_2(T|\lambda) \qquad \text{(IV-17b)}$$

One may similarly construct P-values for X and Y alone.

For $\lambda_x = \lambda_y$

$$P_2(x|T,\lambda_x,\lambda_y) = \frac{1}{P_2(T|\lambda_x,\lambda_y)}\left[1 - e^{-x/\lambda_x} - \frac{\lambda_y}{\lambda_y-\lambda_x}\, e^{-T/\lambda_y} \times \left(1 - e^{\frac{-x(\lambda_y-\lambda_x)}{\lambda_x\lambda_y}}\right)\right] \qquad \text{(IV-18a)}$$

while for $\lambda_x = \lambda_y = \lambda$

$$P_2(x|T,\lambda) = \frac{1}{P_2(T|\lambda)}\left[1 - e^{-x/\lambda} - \frac{x}{\lambda}\, e^{-T/\lambda}\right] \qquad \text{(IV-18b)}$$

In either case

$$P_2(y|T,x,\lambda_y) = \frac{1-e^{-y/\lambda_y}}{1-e^{-(T-x)/\lambda_y}} \qquad \text{(IV-19)}$$

Particularly note that P_{2x} and P_{2y} are independent, and a scatter plot of (P_{2x},P_{2y}) should populate uniformly the unit plane. One test of this which I do use is to calculate

$$C \equiv \frac{\left(N_{<<} - N_{>>}\right)}{\left(N_{<>} + N_{><}\right)} \qquad \text{(IV-20)}$$

Here, $N_{<<}$ is the number of events for which $P_{2X} \leq 1/2$ and $P_{2Y} \leq 1/2$; $N_{>>}$, $P_{2X} > 1/2$ and $P_{2Y} > 1/2$, etc. C is thus a deviate from a multinomial distribution with $\langle C \rangle = 0$.

One may ask why a two-chain formula is needed at all. Using eqn. [IV-10], it would seem that the quantity $\ln P_{1X} + \ln P_{1Y}$, where P_1 is just the one-chain formula, eqn. [IV-12], for the individual potential paths associated with each link (T and T-X, respectively), would be the starting point. The difficulty here is the difference between a priori and a posteriori selection. If one considers all topologies together, irrespective of generation, then either an event-by-event calculation (where an event is a connected topology) or a track-by-track calculation will yield probabilities distributed U(0,1) if the population in fact comes from the hypothesis under which these probabilities are calculated. If the population comes in fact from an alternate hypothesis, the power of these different formulae to discriminate between a hypothesis and an alternate will differ. On the other hand, if one restricts consideration to one particular topology a posteriori, and reject from consideration all other topologies, then one must use formulae specific to the topology in question. This is what has been done with the two-chains.

Consider next the question of the number of interactions, that is, $N(x)$. As already established, $N(x) = N_0(1 - e^{-x/\lambda})$, or identifying N_0 with the fluence Φ

$$N(0 < x \leq X) = \Phi(1 - e^{-X/\lambda}) \equiv \Phi P_1(X|\lambda) . \qquad \text{(IV-21)}$$

It is obvious that at fixed fluence Φ, N obeys a binomial distribution from 0 to Φ with parameter $p = P_1(X|\lambda)$. In particular, consider a contiguous set of distance intervals, $0 < x \leq X_1$, $X_1 \leq x \leq X_2, \ldots$ Suppose the incident numbers of particles was Φ_0, and one observed N_1 stars in the first interval, N_2 in the second, up to N_n in the nth. Let

$$D_1 \equiv X, \quad D_2 \equiv X_2 - X_1 \quad , \ldots, D_n \equiv X_n - X_{n-1} \quad .$$

Further, let

$$\Phi_1 \equiv \Phi_0, \ \Phi_2 \equiv \Phi_1 - N_1 \ , \ldots, \ \Phi_n \equiv \Phi_{n-1} - N_{n-1}$$

Then, one finds immediately that

$$\langle N_n \rangle = \Phi_{n-1} P_1(D_n|\lambda) \qquad \text{(IV-22a)}$$

with an RMS deviation from the binomial distribution,

$$RMS(N_n) = \sqrt{\Phi_{n-1} P_1(D_n \lambda)[1 - P_1(D_n \lambda)]} \qquad \text{(IV-22b)}$$

Since Φ_n are each independent (as the actual observation of the fluence is used), one can obtain the fit of the observations interval by interval, and thus assign an RMS deviate

$$\rho_n = \frac{N_n - \langle N_n \rangle}{RMS(N_n)} \qquad \text{(IV-23)}$$

which for large enough $\langle N_n \rangle$ and $\Phi_{n-1} - \langle N_n \rangle$ is normally distributed.

In the case of the two-chain formula, the situation is more complicated. The second link depends on the first in that the charge of the second is not known until the first has interacted. Hence, one must renormalize. Let

$$P_{21}(n\,\lambda_x, \lambda_y) \equiv P_2(n\,\lambda_x\lambda)/P_1\,n\,\lambda_x$$

Further, let $\Phi(Z_x \to Z_y)$ be the number of tracks of generation n-1 with charge Z_x, which emitted a particle (in generation n) of charge Z_y. One has thus required that Z_x interact and emit Z_y, without requiring that Z_y interact. One is interested in

$$\langle N_{12}\rangle = \Phi(Z_x \to Z_y)\; P_{21}(T\,\lambda_x, \lambda_y) \qquad \text{IV-24}$$

where T is the total potential path from the emission point of the track Z_x. Again N_{12}, the actual number of interactions, obeys a binomial distribution.

However, in any given channel (say, $Z_x \to Z_y$, or in the case of one-chains, Z) at a fixed T, the population may be quite small. To improve statistics, pool the data. Assume that one tests with repeat samples of the same topology and potential paths. Then, letting μ be an index that denotes both the topology and potential path one considers

$$\Phi = \sum_{\mu} \Phi_{\mu}\,, \quad \langle N\rangle = \sum_{\mu} \langle N\rangle_{\mu}\,, \quad N = \sum_{\mu} N_{\mu}\,.$$

Let $p \equiv \langle N\rangle/\phi$; N obeys a binomial distribution from 0 to ϕ with parameter p. Additionally, I will make use of a statistic

$$R \equiv N/\langle N\rangle, \tag{IV-25}$$

which has an RMS deviation obtained from the binomial distribution of N; R has the useful property that $\langle R\rangle = 1$.

The final topic will be estimation of a component λ_a with fraction α. The most events obtain for individual interacting PFs, which of course are one-chains. Hence, one needs to use a modified one-chain formula to obtain P values and likelihood functions. Assuming each track has probability α of having mfp λ_a, one immediately derives

$$P_1(X\ T,\lambda_z,\alpha,\lambda_a) = \frac{(1-\alpha)\left(1-e^{-X/\lambda_z}\right) + \alpha\left(1-e^{-X/\lambda_a}\right)}{(1-\alpha)\left(1-e^{-T/\lambda_z}\right) + \alpha\left(1-e^{-T/\lambda_a}\right)} \tag{IV-26}$$

From this, it is straightforward to calculate the likelihood as the product of the density

$$f(X) = \frac{(1-\alpha)\ \frac{1}{\lambda_z}\ e^{-X/\lambda_z} + \alpha\ \frac{1}{\lambda_a}\ e^{-X/\lambda_a}}{(1-\alpha)\left(1-e^{-T/\lambda_z}\right) + \alpha\left(1-e^{-T/\lambda_a}\right)} \tag{IV-27}$$

for each (X,T) value given the charge Z of the track.

C. Monte Carlo Simulations

All of the preceeding material in this section is a restriction to "exact" statistics, "exact" in quotations because they are in a somewhat idealized world. In all methods depending on the hypothesis $\lambda(Z) = AZ^{-b}$, both this form and the assumption that the exponent b is the same for PFs as VOS occupants is an idealization. In the nonparametric P(F) by laboratory and measured charge, only an assumption of relative homogeneity enters. Finally, one does not in fact construct the Method A results by the rigorous method (total path length up to but not beyond N stars), since one includes all path length observed, including that beyond the last star and one works at finite fluence.

How should one test whether or not these idealizations have any physically significant effect on the results? One possibility is to attempt ever improved analytic approaches. Since the number of physics effects one wishes to include may grow, this would involve a growing complexity of the statistical methods without any necessary gain in one's physical understanding. Another possibility is to use the idealized methods and analyze the results of simulations (which may violate the idealizations) by these methods. In this portion, the latter approach is elected.

A Monte Carlo simulation computer program was written. The output of this program was data in the identical computer format as the actual data of the experiment and hence could be analyzed by the same

programs that were used to otain the results. In addition to testing physical hypothesis, this method gives an additional check on the integrity of the data stream.

The basic component in the simulation is the generation of random interaction distances, assuming that these come from the negative exponential distribution. This is easily done. Let R be a uniform random deviate from 0 to 1 (most FORTRAN compilers have a function to provide these numbers); then $x = -\lambda \ln R$ is an interaction distance for a particle with mfp λ. These x's shall be called SID, Simulated Interaction Distances. SID clearly depends on mfp, and the whole point in the simulation is selecting the mfps (and topologies) in a physical fashion.

Since one wants to simulate something close to the actual data set, the primary interaction distances and topologies (i.e., secondary PF population) actually observed were used. The interaction distances alone will not generate tertiary and later generations unless a topology is assigned at the interaction vertex of the secondary PF. To do this, all observed topologies (actually observed in the experiment, e.g., $O \rightarrow B + Li$, $Ca \rightarrow O + C$, $Ca \rightarrow O + 2\,Li$, etc.) were stored in the computer by charge of the parent; given the charge of the interacting PF, a topology was selected at random. The topology PF $\rightarrow$ no further PFs (all $Z < 3$) was also allowed to occur at random with its measured frequency. In this fashion, simulated events were generated.

A PF was deemed to have interacted whenever its SID was less than its available potential path. SIDs were kept to machine accuracy but were written on the simulated data file rounded off as the original observations. Thus, any error induced by rounding was incorporated. The only remaining question is how to assign mfps to individual tracks.

To incorporate the known systematics into the simulation, the mfp values used were modified. For each true Z, calculated mfps from a realistic geometrical model were used, not AZ^{-b} (Ref. IV-1). Within each true Z, a true mfp was assigned, incorporating isotopic noise; sometimes Z = 8 was given the mfp of ^{16}O, sometimes ^{18}O, etc. To get the true Z from the observed Z (the charge on the data file), an error was selected from the observed Z reproducibility distribution coupled with a systematic bias if so chosen. Thus, both charge misidentification and isotopic noise were included. In fact, the isotopic effects were increased by a factor of 2 for physical robustness; if isotope (Z,A') was predicted to have a 3% change from the VOS occupant of charge Z, a factor of 6% was actually used.

One other feature was incorporated that deserves mention. If one calculates a priori expected mfps based on geometrical models in emulsion, without normalizing to any observed emulsion mfps, (or reaction cross sections from other techniques) one soon discovers that the predicted mfps are much shorter than the observed ones, including observations on primary VOS beams. This is due to detection inefficiencies for certain channels, particularly quasi-elastic reactions at low momentum transfer. One can prove mathematically that if one misses a

constant fraction p of mfp λ_T (the theoretical unnormalized mfp), the observed mfp $\lambda = \lambda_T/(1-p)$ and will obey again an exponential law. This is because at each individual miss one will have a Γ distribution, and the sum of these Γ distributions weighted by their probability (a poisson, since one in principle can have an infinite number of misses), recovers an exponential of parameter λ. To simulate this, P = 0.5 was actually assumed, i.e., emulsion is 50% efficient. After selecting a mfp as explained above (including charge assignment and isotopic effects), this value was divided by two and then generated an SID. If this distance were within the stack, another random number was generated. If it were less than 0.5, a detected interaction was assumed to have occurred; if not, another SID using the same $\lambda/2$ was generated and the program proceeded in like fashion until the "particle" suffered a detected interaction or left the stack.

In this fashion, many pseudo-copies of the data were generated. Each copy was fed through the analysis program package and pseudo-results generated. I shall briefly present the results of all these put together, first for Method A and then Method B.

1) Method A. The P(<F) distribution by lab, charge, and distance cut at 2.5 cm is fig. IV-1. $\bar{P} = 0.50 \pm 0.02$ with an RMS deviation of 0.296 ± 0.012; both are within limits of $\langle P \rangle = 1/2$ and $\langle RMS \rangle = 1/\sqrt{12}$. Similarly, results for Λ^*(D) and Λ^* (Generation) agree with expectations.

2) Method B. Here again, things are as expected. For illustration, examine the $P_2(S)$ distributions and likelihood curve. $\bar{P}_2 = 0.50 \pm 0.02$; the average likelihood curve is displayed in fig.

IV-2. It peaks at $\Lambda^{\star} = 29.6$, with rms deviations as illustrated.

In all cases, a "normal" simulation, using conventional nuclear physics and the systematics, produces normal physics. It gives results in accord with the observations (as a fluctuation) with the probabilities assigned. Hence, one seems compelled to conclude that the statistical methods presented above are valid for a physical understanding of the data.

V. Results

A. Method A

The first result to present is the MFP parameter Λ^* of secondary and later generation PFs as a function of distance after emission, i.e., method A'. These are calculated under the assumption that $\lambda = \Lambda Z^{-b}$ with b = 0.44 for LBL data and b = 0.43 for NRC data. The error bars assigned represent one standard deviation assuming the primary beam value. Thus, if one observes $\Lambda^* = 20$ cm with 100 stars and one supposes $\Lambda = 30$ cm, then (in the approximation to which $\sqrt{N}$ statistics apply) one quotes $\Lambda^* = 20 \pm 3$ cm, <u>NOT</u> $\Lambda^* = 20 \pm 2$ cm. This is because it is assumed at the outset that all PFs should have the mfp parameter Λ as measured on primary beams.

To plot the results of two independent experiments with different values of Λ ($\Lambda_{LBL} = 32.3$ cm, $\Lambda_{NRC} = 28.9$ cm), one must either have the weighted mean value Λ (to be expected) change as function of distance (since at different distances after emission the contribution of the two experiments changes; e.g., all the data beyond 12 cm are from NRC), or renormalize to a constant mean value taken as $\Lambda = 30.4$ cm. For simplicity of display purposes, the latter has been done. The result is fig. V-1.

Note the apparent lowering of Λ^* for the first several cm and the consistency with the primary VOS beams value at distances larger than 5 cm. One may ask: Is this an artifact caused by the power law

fit and/or the intermixing of data from the two experiments? To test whether this result is physically significant, one must circumvent the possible erroneous conclusions induced by the use of the parametrization and also view the results independently from the two experiments. One thus examines the data charge-by-charge from each of the two laboratories separately. To maximize the utilization of the information, the data are broken into two groups,

$$\lambda^*_< \equiv \lambda^*_{Z,LAB}(0 < D \leq 2.5 \text{ cm}), \lambda^*_> \equiv \lambda^*_{Z,LAB}\ (D > 2.5 \text{ cm})$$

The distance of 2.5 cm has been chosen partly for convenience and partly for physical reasons. Since the maximum likelihood fit to the data assuming just one short mean free path component predicts that component to have a mean free path of 2.5 cm, this seems like a logical distance at which to divide the data sample.

To perform the test, take $F_{Z,LAB} = \lambda^*_< / \lambda^*_>$; one knows the number of stars $N_<$ and $N_>$ observed by charge and lab and can thus compute a P for the observation on the assumption that $\lambda^*_<$ and $\lambda^*_>$ are from the same population. One then histograms the resulting P values; recall that <u>if these $\lambda^*_<, \lambda^*_>$ values are from the same population, the P values must be distributed uniformly from 0 to 1</u>. The observed result is fig. V-2a. The cross-hatched area represents the six charges from NRC, and the remaining area is the 24 charges from LBL. It is immediately obvious that the distribution is sloping towards low P values; the values of P have been calculated such that this corresponds to $\lambda^*_< < \lambda^*_>$. As a statistic, the mean P has the value 0.323, calculated

from the unbinned $\overline{P}$ values; one expects $\langle P \rangle = 1/2 \pm 1/\sqrt{360}$. Thus, the observed $\overline{P}$ is -3.4 standard deviations from $\langle P \rangle$, a difference exceeded with one-sided probability 3×10^{-4}.

Based on this result, there are fewer than three chances in 10^4 that the $\lambda^*_<$ values come from the same population, charge-by-charge and lab-by-lab, as the $\lambda^*_>$, values. It is reasonable to conclude that they are significantly shorter and that the low values of λ^* at short D is not an artifact. More important for its physical implications, this result is independent of many systematic problems that potentially plague other methods. It only assumes relative homogeneity of the PF flux, as traditional isotopic effects should by no means cause such an observation. Thus, one seems compelled to conclude that there is something peculiar about the mfps of PFs within the first few cm after emission.

The simplest assumption to explain this result is that in addition to PFs with "normal" mfps, there is another species present with mfp λ_a and with fraction of all PF flux α. One thereby assumes that λ_a and α are independent of Z, which may be an oversimplification. By procedures explained in Sect. IV B, one finds $\lambda^*_a \approx 2.5$ cm and $\alpha \approx 0.06$. To calculate the expected Λ under this model, one can reasonably replace all random variables by their expectations. Thus,

$$\langle \Lambda \rangle_\Delta = \frac{\sum_Z \Phi^\Delta_Z \left[(1-\alpha) P^\Delta_Z \lambda_Z + \alpha P^\Delta_a \lambda_a \right] Z^b}{\sum_Z \Phi^\Delta_Z \left[(1-\alpha) P^\Delta_Z + \alpha P^\Delta_a \right]} \qquad \text{(V-1)}$$

where Δ is the interval $D_1 < D \leq D_2$, Φ^Δ_Z is the population of charge

PFs of Z incident on Δ, $\lambda_Z = \Lambda_{BEAM} Z^{-b}$, $P_Z^{\Delta} = e^{-D_1/\lambda_Z} - e^{-D_2/\lambda_Z}$ and $P_a^{\Delta} = e^{-D_1/\lambda_a} - e^{-D_2/\lambda_a}$. The result for $\langle\Delta\rangle$ is depicted as the smooth curve in fig. V-1; as can be seen it agrees well with the observations. The reason this effect has been termed anomalous is first seen here. If one attempts to increase λ_a to, say, 10 cm, there is no value of α that will well reproduce the observations. They seem to require the existence of a component of the PFs produced with a few per cent probability, with mfps outrageously shorter than any of the primary beams employed. A value of 10 cm is already ludicrous, considering that this implies a charge in the calcium range among PFs from oxygen! A 2.5 cm component is probably a shorter mfp (i.e., larger cross section) than that of uranium. This suspected component of PFs has been dubbed "anomalons".

If the short mfp is due to the cooperative effect of a few baryons (a "damaged zone") bound to a normal nuclear fragment, one could understand the approximate independence of λ_a from charge.

Suppose the "λ" of the damaged zone were λ_w; then

$\lambda_a \approx \frac{1}{(1/\lambda_w + 1/\lambda_z)}$. If $\lambda_w = 3.5$ cm and $\lambda_{Z=26} = 7$ cm,

then $\lambda_a \approx 2.3$ cm; while for $\lambda_{Z=3} = 18$ cm and the same λ_w, $\lambda_a = 2.9$ cm. Thus, for nuclides from Fe to Li, the equivalent anomalon λ_a would change from 2.3 cm to 2.9 cm, a difference which is undetectable with the present data. While the assumption of a damaged zone and a one-component anomalon is probably too crude in every detail, it does reproduce the overall observations.

Another way to examine the data is to pool them within some charge bin and not use Z^b as a length weighting factor. This has been done for $3 \leq Z \leq 8$, where both laboratories contribute, and also $9 \leq Z \leq 16$ and $17 \leq Z \leq 26$, where only L3L data are available. One obtains $\bar{\lambda}^*_<$ and number of stars and similarly $\bar{\lambda}^*_>$, as indicated in Table V-1. For comparison, the prediction from $30.4\ Z^{-0.44}$ cm is presented, this being the average fit to both NRC and LBL primary VOS beam data. The pooling was done by summing total path length observed within the distance interval and charge interval and dividing this by the number of stars. Again, inspection of Table V-1 reveals that at distances within 2.5 cm of emission PFs have short mfps, while at longer distances, primary beam expectations are essentially fulfilled. Comparing the values of Λ^* assuming $\lambda_Z = \Lambda_Z^{-0.44}$, one obtains $\Lambda^*(\leq 2.5\ \text{cm}) = 25.0$ cm with 536 stars and $\Lambda^*(>2.5\ \text{cm}) = 30.0$ with 924 stars. These estimates are 3.3 standard deviations apart, having a $P(<F)$ of 5 (10^{-4}).

In addition to a comparison by distance after emission, one may also wish to compare particles by generation. Primary beam nuclei do not have a short mfp component, while their progeny seem to evidence one. Is this effect independent of generation (starting with the secondary) or does it change with different PF generations? For example, if the "damaged zone" idea is on the right course, such a zone might persist through several generations, decreasing the average mfp in later generations.

To test this, compare secondary PFs with tertiary and later generation PFs. Start with the $P(<F)$ by lab and charge method. Here one

computes $F_{GEN} = \lambda^*_{\geq 3}(Z,\mathrm{lab})/\lambda^*_2(Z,\mathrm{lab})$ where the subscript denotes generation; the histogram of P values is fig. V-2b. There are six charges at NRC and twenty-three at LBL (there were not enough tertiary tracks in one charge to obtain any stars). For 29 events, P = .387, with $\langle P\rangle = 1/2 \pm 1/\sqrt{348}$, so P is equivalent to -2.11 SD. However, the highest P value recorded is 0.778; the binomial probability to observe 0 events in the uniform distribution, out of 29 attempts, with p = 0.778 is $?(10^{-4})$. Hence, the mere presence of no value of $P(\langle F_{GEN}) > 0.778$ is rather unusual, as one would have expected about six events.

This also appears to some extent in the values of λ^* by generation. Secondaries have λ^*_2 = 28.8 cm, 1196 stars, while later generations have $\lambda^*_{\geq 3}$ = 25.2 cm, 264 stars. This has a probability of about 0.03 to occur. On the face of things, it seems that $\lambda^*_{\geq 3} < \lambda^*_2$, which would be indicative of a retained property or a larger admixture of anomalons in later generations. I shall return to this topic in Section V B.

B. Method B

After having observed an apparent shortening of Λ^* in the first several CM, as calculated by Method A, turn attention to "Method B", giving consideration to interacting PFs only.

First consider all interacting tracks within the context of the one-chain formula, eqn. IV-12. In the data, there are 1460 PF stars, and assuming that λ_z has the values predicted by the LBL and NRC fits to primary VOS beams, one obtains the $P_1(X \quad T, \quad , b, LAB)$ histogram in fig. V-3. $\overline{P}_1 = .469 \pm 1/\sqrt{17520}$. This corresponds to -4.1 standard deviations, with a probability of $2 \cdot 10^{-5}$.

The logarithmic likelihood curve of these data is displayed in fig. V-4; the peak is at $\Lambda^* = 22.8$ cm. The primary beam value is down three orders of magnitude on the likelihood curve. Furthermore, the same data (now including noninteracting tracks) within the context of Method A yields $\Lambda^* = 28.2$ cm, which is down by more than two orders of magnitude on the likelihood curve. Thus, $\Lambda^*_B < \Lambda^*_A$. However, one normally expects these two estimates to be consistent. One may demonstrate this physically by reference to fig. V-5, where the NRC primary ^{16}O likelihood curve and the Method A result is displayed.

Since all tertiaries that do interact come from a secondary that also interacted, one may profitably use the two-chain formula. For $Z \geq 3$, there are 215 secondary-tertiary two-chains. In fact, there are 221 cases of tertiary stars, which means there are a few "forks". In this instance, I arbitrarily select one of the branches at random, thus converting a fork geometry to chain geometry.

Consider the likelihood curves for λ given the observed X, Y, and S = X + Y measurements for each event, fig. V-6. As can be seen, secondaries that gave a tertiary that interacted have $\lambda_X^* = 21.8$ cm, tertiaries have $\lambda_Y^* = 18.2$ cm, and $\lambda_S^* = 19.8$ cm. An examination of the likelihood curves reveals that none reject the primary beam value; before accepting this conclusion, one should examine the P distributions. Histograms of $P_2(S)$, $P_2(X)$, and $P_2(Y)$ are fig. V-7. $\bar{P}_2(S) = 0.444$ with 215 events, which is equivalent to -2.84 SD. As a different point of view, one can look at $\bar{P}_2(X) = 0.465$ and $\bar{P}_2(Y) = 0.463$, both of which are below $\langle P \rangle = 1/2$ but each only about -2 SD, which is not an outrageous fluctuation. However, if one plots the $P_2(X)$ distribution against the $P_2(Y)$ distribution, an interesting observation emerges.

$P_2(X)$ and $P_2(Y)$ are independent as these quantities have been here calculated, and thus a scatter plot of $P_2(X)$ against $P_2(Y)$ should populate uniformly the unit plane. The result is shown in fig. V-8, where the data are binned in intervals $0 < P < 1/2$, $1/2 < P < 1$ on both axes. One constructs C [eqn. IV-20] which has the value (75-46)/(47+47) = 0.3085; however, $\langle C \rangle = \pm 0.0975$, so the observed value corresponds to 3.1 SD from the expectation. This is the first clear hint of "memory", by which one means that a "short" PF gives rise to "short" progeny. What is observed is that a low $P_2(X)$ value gives rise to a low $P_2(Y)$ value. This may be illustrated in a different way. Suppose one examines $P_2(Y)$ as a function of $P_2(X) \leq 1/2$ or $> 1/2$. Since $P_2(X)$ is independent of $P_2(X)$, one expects $\langle P_{2<}(Y) \rangle = \langle P_{2>}(Y) \rangle = 1/2$, and

similarly for $P_{2<}(X)$ and $P_{2>}(X)$; here the subscript "<" refers to the $\leq$ 1/2 cut on the <u>other</u> P_2 variable, and ">" to the > 1/2 cut. One obtains:

$\bar{P}_{2<}(Y) = .428$, 122 stars; $\bar{P}_{2>}(Y) = .509$, 93 stars

$\bar{P}_{2<}(X) = .435$, 122 stars; $\bar{P}_{2>}(X) = .502$, 93 stars

If taken at face value, hence that one is not merely looking at an unusual fluctuation, interpretation of this result has several physical consequences. First, it strongly speaks against isotopic effects and related classical nuclear physics. If this were the root cause of the effect, one would not expect that $\bar{P}_{2>} = 0.5$ in both cases; even though the fit AZ^{-b} cannot be exact, these PF data do not viciously reject such a fit, as one symptom of a rejection would be $\bar{P} \neq 1/2$.

Recall $\bar{P} < 1/2$ indicates short MFPs relative to the primary beam fit and that P_2 <u>removes</u> any bias generated in either X or Y by the requirement that both links in the two-chain interact. As a second point, a short X seems to give rise to a short Y. If "anomalons" exist, then an anomalon parent tends to enhance the chance of an anomalon progeny.

Third, the fact that $\bar{P}_{>}(Y)$ does not significantly differ from 1/2 indicates that the seemingly "normal" $P_2(X) > 0.5$ secondary population does not produce anomalous tertiaries as copiously as normal primaries produce anomalous secondaries. One possible explanation would be the existence of an energy threshold for production; this is also suggested by some of Judek's cosmic ray observations[V-1]. If so, the threshold must be about 1.7 A GeV.

Before leaving the subject of likelihood curves, I shall estimate the fraction α of a λ_a component, and λ_a itself simultaneously using all 1460 interacting PFs. The likelihood is now displayed as contours in fig. V-9 for $\alpha^* = 0$ to 0.5, $\lambda_a^* = 0.1$ to 20 cm. The peak is at $\lambda_a^* = 2.5$ cm, $\alpha^* = 0.06$.

As a consistency check, consider the N(X) distributions, eqn. IV-21. While one can analyze the data using each track and its potential path (where now one includes both interacting and noninteracting tracks; for noninteracting tracks T is the distance actually followed), it is much more intelligible to perform the analysis at fixed T. To fix T, demand each track could have gone <u>at least</u> T cm, even if it interacted within T. The N(X) distributions for T = 3 and T = 9, summed over all PFs, are displayed as fig. V-10. To assess the statistical significance of this observation, examine the T = 3 result. There are 2386 incident PFs, and one expects 504.3 stars assuming the fits to primary beams. In the data, there are actually 581 stars. Crudely, an rms deviation is $(581-504.3)/\sqrt{504.3} = 3.4$; more exactly, using repeat samples of identical charge composition, one has 3.85 rms deviations from the binomial distribution. For comparison, I also display in fig. V-10 the fits with $\alpha = 0.06$, $\lambda_a = 2.5$ cm. As is obvious, the fit is again quite good.

VI. Conclusions

If one accepts things from a purely statistical view and accepts the assumption that $\lambda_Z = AZ^{-b}$ as fit to primary VOS beams, there are fewer than five chances in 10^5 that all PFs could have these mfp values. This is based on the one-chain formula applied to all PFs; additionally, the lowering of P_1 indicates a short mfp, as shown by the likelihood curve.

From a more physical point of view, the test within the context of Method A treating each laboratory separately by charge (thus avoiding assumptions about just what values should be obtained for λ_Z) gives fewer than five chances in 10^4 that the mfp is constant as a function of distance after emission. One can fit the data by assuming that 94% of PFs have λ_z as given by the fit on primary beams and that 6% of PFs have $\lambda_a = 2.5$ cm, independent of Z. This λ_a corresponds to a conventional nuclear reaction cross section on the order of or larger than uranium.

Taken literally, the results imply the existence of a new state of multibaryonic matter with a hadronic reaction cross section three to ten times larger than the normal VOS occupant of the same charge. However, before reaching such a profound conclusion, one must exhaust all other possible avenues of interpretation.

The obvious conclusion is that one is dealing with a systematic error. A trivial systematic, such as the incorrect assignment of interaction distances or potential paths, is ruled out by the internal checks and remeasurements. Likewise, the data stream was checked

against the scanner's original notes and scan sheets. In every case, all computed quantities (such as S_N/N) were stable to at least four significant figures. The Monte Carlo simulation also incorporated this same rounding (to 100 μm units) without pathological consequences.

A potentially more troubling systematic is the charge measurement algorithm. For distances on the order of 1 mm or larger, the observed statistical error of ±1 charge should be adequate. For shorter distances, the charge balance method was used, which requires detection of all relativistic singly charged tracks and correction for both meson production and charge exchange. As an alternative, one can discard all track lengths (interacting or not) less than some cutoff distance and examine the significance of the results. For cuts less than 5 mm (20 fields of view at 500 magnification!), neither the Method A nor B results change.

One may further query as to the energy spectra assumptions. This has little effect since above ≈500 A MeV, total reaction cross sections are remarkably constant[VI-1]. If anything, inclusion of such tracks would bias the data against a short mfp effect. Considering the beam kinetic energy is ≈2 A GeV, slower tracks would have a higher specific ionization[VI-2] and thus a larger apparent charge. Such a larger charge would be presumed to have an intrinsically shorter mfp. Besides, the charge measurements showed no tracks were significantly slowing.

A standard concern is differential scanning efficiency. In this scenario, an observer detects events more efficiently at short track lengths than at longer distances. To counter this, note that one ob-

serves the "correct" mfp at "long" distances and sees an excess number of interactions at short distances. LBL has rescanned and examined the interactions; they are really there. Furthermore, as already mentioned, the LBL rescan showed no differential efficiency. The other possibility is that all primary beam measurements are in error; but here, too, cross checks have not discovered any such errors.

The possibility of gross defects or inhomogeneities in the emulsion composition itself must also be examined. LBL and NRC used two separate pours; that both could be identically defective seems absurd. Moreover, one can perform internal checks on this. Such gross defects would affect the sensitivity, the charge measurement, and the primary mfp. This was <u>not</u> observed. Additionally, such effects would correlate with absolute positions in the plates, rather than relative distances after a star; this also was not seen.

The next possibility for a conventional effect would be real background stars. These would have two sources: random background from radioactive contamination and neutron spatter and correlated background from either a neutron or low-Z track situated directly on top of another track. For high-Z PFs, Coulomb repulsion must force the two tracks apart. In either case, a cut at 5 mm should have eliminated the effect; as mentioned above, it does not. As a further check, a background interaction as defined above must appear as a charge change of the PF at the vertex of 0 or 1. The maximum charge change that was used from NRC was 8 - 3 = 5. As a test, consider R [eqn. IV-25] for the two-chain formula for secondary-tertiary two-chains as a function of the secondary charge minus the tertiary charge

(the charge change ΔZ). One may think that this depends on the branching ratio for ΔZ, but since one normalizes to those possible secondary tertiary 2-chains of the same ΔZ, it does not.

For $0 \leq \Delta Z \leq 1$, there are 118 possible two-chains, one expects 59.1 tertiary stars, and 74 are observed, so $R = 1.25 \pm 0.092$; for $2 \leq \Delta Z \leq 5$, 164 possible, 65.2 expected and 84 observed, so $R = 1.29 \pm 0.0986$. Thus, in the potential "background" channel ($0 \leq \Delta Z \leq 1$) R has a value that agrees quite well with the value in the "non-background" channel. Incidentally, converting both of the values of R to an rms deviation [(R - 1)/RMS(R)] and then summing the squares, $\chi^2 = 16.5$, 2 DOF, which is equivalent to 3.5 SD. As a further note, this argues against β emitters decaying in flight, which would also appear in the $0 \leq \Delta Z \leq 1$ cut.

Since there are no indications for background or coincident stars, I conclude the search for possible conventional effects with those that would simulate nuclear interactions but that are not. The first obvious candidate is hypernuclear decay in flight (along with β-delayed proton emitters and such similar states); this seems appealing in that $c\tau \approx 3$ cm corresponds with hypernuclear lifetimes. Unfortunately, hypernuclear production cross sections have been measured and are much too small at the energies of these experiments to account for the observations.[VI-3] Additionally, these "decay in flight" stars would appear as pure projectile fragmentations without any target prongs (so-called $N_H = 0$ stars). The fact that one does not observe a relative fractional excess in the $N_H = 0$ channel argues against this. By a similar argument, one can eliminate nuclear π^- capture from a pionic atom

(a PF that has a π^- in an atomic orbital in the PF rest frame), which again would appear as a pure projectile fragmentation. As for π^- atoms interacting in flight, where either the orbital π^- or its binding PF interacts with the emulsion, one would again expect the effect to be enhanced in the $\Delta_Z \leq 1$ channel. The fact that other channels display the abnormality argues against this.

The last conventional possibility is a normal nuclear excited state with a lifetime $c\tau \gtrsim 5$mm. Such a state would γ decay to ground, say, and while in an excited state would have a larger reaction cross section.

This explanation fails on numerous accounts. First, most isotopes will be in their ground states; isotopes alone would not produce the P(<F) by laboratory and charge histogram since the "length scale" of such effects would be >>2.5 cm (rather on the order of $\approx$ 10 cm). Second, one can calculate rms radii to the next shell model orbital (for an orbital excitation) and then integrate the resulting density to get effective excited state cross sections; the changes are less than 10%. Moreover, the overwhelming majority of long-lived nuclear excited states that could affect these observations involve angular momentum recoupling rather than orbital promotion, and for these the reaction cross section change can be calculated to be quite small. The results would require $\approx$100% of all PFs to be produced in isotopic excited states with reaction cross sections > 20% larger than the VOS occupant of the same charge and then to decay back to ground with a mean $c\tau \approx 3$ cm. Even granting this, which seems very unlikely, it fails to account for the observation that a short secondary PF gives

rise to a short tertiary PF. There should be no relationship of this sort if isotopic excited states were the cause.

Let me summarize the findings:

1) The P(<F) distribution by lab, charge, and a 2.5 cm cut, rules out a homogeneous sample. To explain this result would require isotopic excited state reaction cross sections much more deviant from conventional predictions than can be accommodated.

2) Such extreme proposed isotopic explanations would not explain the observations on the relation between short tertiary links and short secondary links in two-chains and would also be very hard pressed to reproduce the $\Lambda^*(D)$ curve by method A'.

3) Systematic and background effects can be essentially eliminated by the observations themselves (normal Λ^* at large distances, no outrageous relative enhancement of the $\Delta Z \leq 1$ channel, etc.) and by the checks for potential problems arising from the scanning and measuring techniques.

One is thus left in a predicament. Conventional nuclear physics and sytematics fail to explain the observations. The statistical probability that one is dealing with a fluctuation is $\lesssim 5(10^{-4})$. The existence of a new type of multicharged, presumably multibaryon, state with a hadronic reaction cross section between three and ten times that of a VOS ground state nuclide of the same charge would explain the observations. However, it is impossible to accommodate such a state with a lifetime $c\tau \gtrsim 5$ cm within the context of conventional nuclear physics. I must add that with the present statistics, one does not know precisely

how many anomalous components are present nor their exact properties. The evidence does argue strongly for the existence of at least one component of PFs with a reaction mfp considerably shorter than anything accepted within conventional nuclear physics.

To elucidate the exact nature of the phenomenon will require more data and further experiments. The obvious questions concern the mass, lifetime and decay mechanism for this presumed component. One is interested in knowing its production mechanism; e. g., does it require that both participants in the collision be multi-baryonic, or will p-A collisions give the same effect? By obtaining some insight into the answers to these sorts of questions, one can presumably build a triggered device to address further details of the phenomenon. It is clear that with the present data, and further data of the same sort but with somewhat better statistics, the evidence for the existence of such new forms of matter must remain circumstantial. It is also clear that no matter how strong the circumstantial evidence may eventually become, a result potentially as profound as this must ultimately rest upon more direct observations.

Acknowledgements

It is always difficult when writing a document of this sort to properly give all the persons involved with it all the recognition they deserve. Indeed, the continuous process of growth and change is mitigated by many circumstances and individuals. Still, several people of special merit deserve credit here.

The first two of these are Dr. Harry Heckman and Dr. Erwin Friedlander. It was Erwin Friedlander who first brought the rather well kept secret of a short mean free path component to my attention; this seriously piqued my attention, espcially in that I had phenomenologically predicted just such a possible behavior for a new state of nuclear matter which, of course, could not exist. Harry Heckman provided much encouragement and leadership while the data were slowly being accumulated and new methods of analysis were being developed, and enabled me to obtain the experimental tools and training needed.

Next, I must thank Prof. Joseph Cerny. He first revealed to me that there is more to the strong interaction than elementary particle physics, and that the physics of multibaryon bound states also has things to offer.

I must also thank Dr. Norman Glendenning who offered me succor during the initial stages of my professional activities, and graciously permitted me to get involved with the experimental details of this work, as much outside of his normal sphere as it was.

I also must mention my principal campus liason, Prof. John Rasmussen. Over the years, he has given much useful advice and invested many hours of his time.

Last, but certainly not least, I mention my mother, Mrs. Viola Karant. Her endurance of a physicist about the house, showing interest in things she never understands, and never understanding how so much work seems invested in a field with no practical applications, all of this and more, deserves much greater recognition than is even possible here.

As for the many people involved in the details of this project, and its ongoing effort, only a few can get the credit here they so justly deserved. First, there is Dr. Barbara Judek, who adhered to her experimental observations despite what others might believe, and who graciously provided much of the data herein used. Second, I must gratefully acknowledge the two scientific data analysts, Ms. Hester Yee and Mr. Roy Gimpel, whose combined effort made much of this investigation possible. Third, the technical assistance given by Mr. Henry Dykman and Mr. James Hodges is gratefully acknowledged, as are the contributions of the Bevalac operations staff.

This work was supported by the Director, Office of Energy Research, Division of Nuclear Physics of the Office of High Energy and Nuclear Physics of the U.S. Department of Energy under Contract Number DE-AC03-76SF00098

References

There are two notes which must be given here: (i) This work is an outgrowth from results published in Evidence for Anomalous Nuclei among Relativistic Projectile Fragments from Heavy-Ion Collisions at 2 GeV/Nucleon, E. M. Friedlander, R. W. Gimpel, H. H. Heckman, Y. J. Karant, B. Judek, and E. Ganssauge; (ii) the reference Barkas refers to the treatise Nuclear Research Emulsions, Vol. I, by W. H. Barkas, Academic Press, 1963.

I-1. A. Malone, Nuovo Cimento Suppl. 12, 353 (1954); S. Tokunaga, T. Ishii, and K. Nishikawa, Nuovo Cimento 5, 517 (1957); E. M. Friedlander and M. Spirchez, Nucl. Sci. Abstr. 15, 347 (1961); B. Judek, Can. J. Phys. 46, 343 (1968); T. F. Cleghorn, P. S. Freier, and C. J. Waddington, Can. J. Phys. Suppl. 46, 572 (1968). B. Judek, Can. J. Phys. 50, 2082 (1972).

I-2. H. H. Heckman, D. E. Greiner, P. J. Lindstrom, and H. Shwe, Phys. Rev. C 17, 1735 (1978) and present work.

I-3. B. Judek, in Proceedings of the Fourteenth International Conference on Cosmic Rays, 1975, edited by Klaus Pinkau (Max-Planck-Institute, Munchen, 1975), Vol. 7, p. 2342; and private communication.

II-1. Barkas, Chap. 3.5

II-2. J. Jaros, A. Wagner, L. Anderson, O. Chamberlain, R. Z. Fuzesy, J. Gallup, W. Gorn, L. Schroeder, S. Shannon, G. Shapiro, and H. Steiner, Phys. Rev. C 18, 2273 (1978); see also Ref. I-2.

II-3. H. C. Bradt and B. Peters, Phys. Rev. 77, 54 (1950).

II-4. P. J. Karol, Phys. Rev. C 11, 1203 (1975).

III-1. D. E. Greiner, P. J. Lindstrom, H. H. Heckman, B. Cork, and F. S. Bieser, Phys. Rev. Lett. 35, 152 (1975). Note that these results were not reported in the lab frame, so that a Lorentz transformation is involved to obtain the result quoted.

III-2. H. H. Heckman, et al., loc. cit.

III-3. Barkas, Chap. 8.4.

III-4. Ibid., Chap. 8.10.

III-5. D. E. Greiner, et al., loc. cit.

III-6. Barkas, Chaps. 9 and 10.

IV-1. P. J. Karol, loc. cit.

V-1. Ref. II-1, Judek (1972).

VI-1. J. Jaros, et al , loc. cit.

VI-2. Barkas, Chap. 9.

VI-3. K. J. Nield et al., Phys. Rev. C 13, 1263 (1976).

Table V-1. Mean estimates for the mean free path λ and the parameter Λ (Eq. II-3) at different distances D from the origins of PF's for grouped charges. Expected values assuming Eq. II-3 are given in the last column.

Z	$\bar{\lambda}^*(D \leq 2.5$ cm) (cm)	$\bar{\lambda}^*(D > 2.5$ cm) (cm)	$\langle\bar{\lambda}\rangle$ (cm)
3-8	12.4 ± 0.7	14.0 ± 0.5	14.6
9-16	8.3 ± 0.7	11.6 ± 1.0	10.6
17-26	6.0 ± 0.6	8.0 ± 0.8	8.4
	$\Lambda^*(D \leq 2.5$ cm) (cm)	$\Lambda^*(D > 2.5$ cm) (cm)	$\langle\Lambda\rangle$ (cm)
3-26	25.0 ± 1.1	30.0 ± 1.0	30.4

Figure Captions

Fig. II-1 The mean free path $\lambda(Z)$ versus Z. The large circles with error bars are the LBL observations on primary beams; the large triangles with error bars are the NRC primary observations. The small circles are fitted theoretical predictions; the appearance of multiple circles for the same Z represents istotopes of different A. The straight line is $30.4\ Z^{-.44}$ cm, which represents the "average" fit to both data sets combined.

Fig. III-1ab The observed charge measurement reproducibility for NRC and LBL. Below the NRC observations are plotted the mean N_δ (number of δ-rays) per mm to which the charge in question corresponded in one of the ways NRC determined charge.

Fig. III-2ab The calculated lab frame kinetic energy distribution of PFs at NRC and LBL by generation.

Fig. IV-1 The histogram of the P(F) distribution by lab, charge, and 2.5 cm distance cut from repeated independent samples of the Monte Carlo simulation. Since each individual P value is represented, the distribution should be U(0,1).

Fig. IV-2 The normalized likelihood curve for the parameter Λ (eqn. II-3) assuming b = 0.44 derived from the $P_2(S)$ distribution (eqn. IV-17ab) from repeated independent samples of the Monte Carlo simulation. The error bars represent the observed RMS deviations for each value from the repeated samples.

Fig. V-1 Estimates Λ^* for the parameter Λ (eqn. II-3) at different distances D from the origins of PFs: full circles, experiment; dashed line, prediction from Λ_{beam}; solid line, prediction assuming a 6% admixture of PFs with λ_a = 2.5 cm.

Fig. V-2 Experimental frequency distribution of (a) $P_D(F_D)$ and (b) $P_{gen}(F_{gen})$; see text; the dashed line is the expected U(0,1) distribution; the points with error bars are the experimental means $\overline{P}$, to be compared to their expectation $\langle P \rangle = 1/2$; the shaded area refers to the results from NRC.

Fig. V-3 The experimental frequency distribution of $P_1(X)$, eqn. IV-12. The histogram is the data. The solid vertical line is the expected value for the mean $\overline{P}$, $\langle P \rangle = 1/2$, while the solid circle is the observed value of $\overline{P}$; the error bars on $\overline{P}$ are the size of the solid circle. The dashed line is the expected U(0,1) distribution.

Fig. V-4 The normalized likelihood curve for the parameter Λ (eqn. II-3) from the same data as in Fig. V-3.

Fig. V-5 The normalized likelihood curve from the $P_1(X)$ distribution (eqn. IV-12) for the parameter λ from the NRC primary ^{16}O data. For comparison purposes, the value of the Method A estimator, λ_A^*, is also shown by the arrow. As can be readily seen, the two methods give consistent estimates.

Fig. V-6 The normalized likelihood curves for the parameter λ from the experimental X, Y, and S distributions (eqns. IV-18ab, IV-19, IV-17ab, respectively). The dashed line is the result from the X distribution, the dotted line is the result from the Y distribution, and the solid line is the S distribution (compare to Fig. IV-2, where the S distribution Monte Carlo simulation result is displayed). The curves have been displaced slightly at the peak for clarity.

Fig. V-7 The same data as in Fig. V-6, but now examined from the P distributions (which should be U(0,1)).

Fig. V-8 The scatter plot of the $P_2(X)$ distribution versus the $P_2(Y)$ distribution as given in Fig. V-7.

Fig. V-9 Normalized likelihood contours for the parameters λ_a and α (eqn. IV-27) from all 1460 one-chains, assuming the primary beam fits as given in Chap. II. The cross marks the maximum likelihood estimate.

Fig. V-10 Distributions of interaction distances x for events with potential paths $T \geq T_1$; dashed and solid lines have the same meaning as in Fig. V-2.

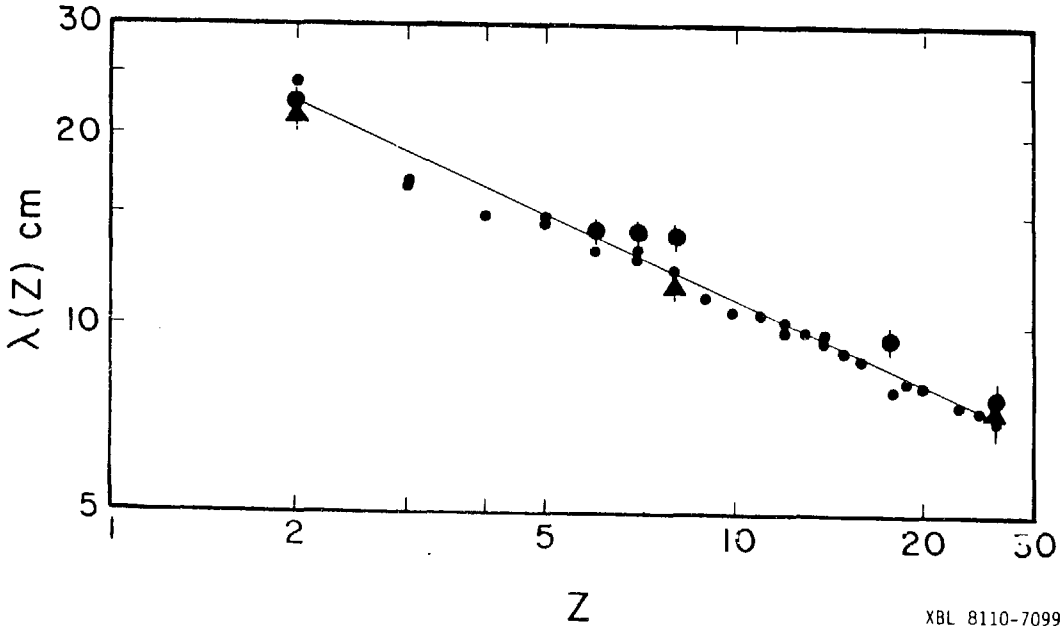

XBL 8110-7099

Fig. II-1

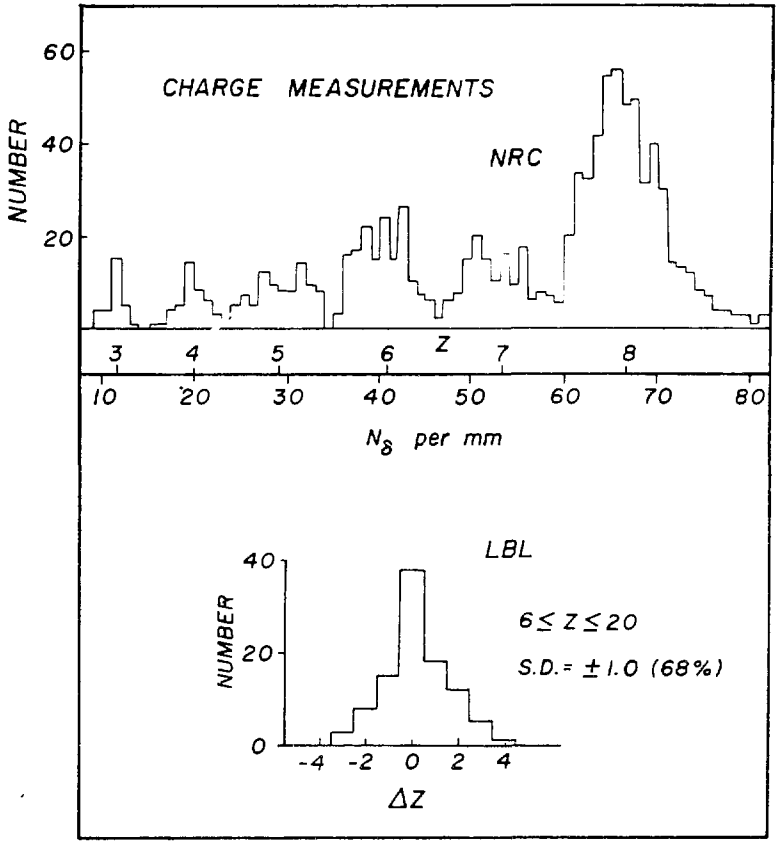

XBL 8110-7096

Fig. III-1a,b

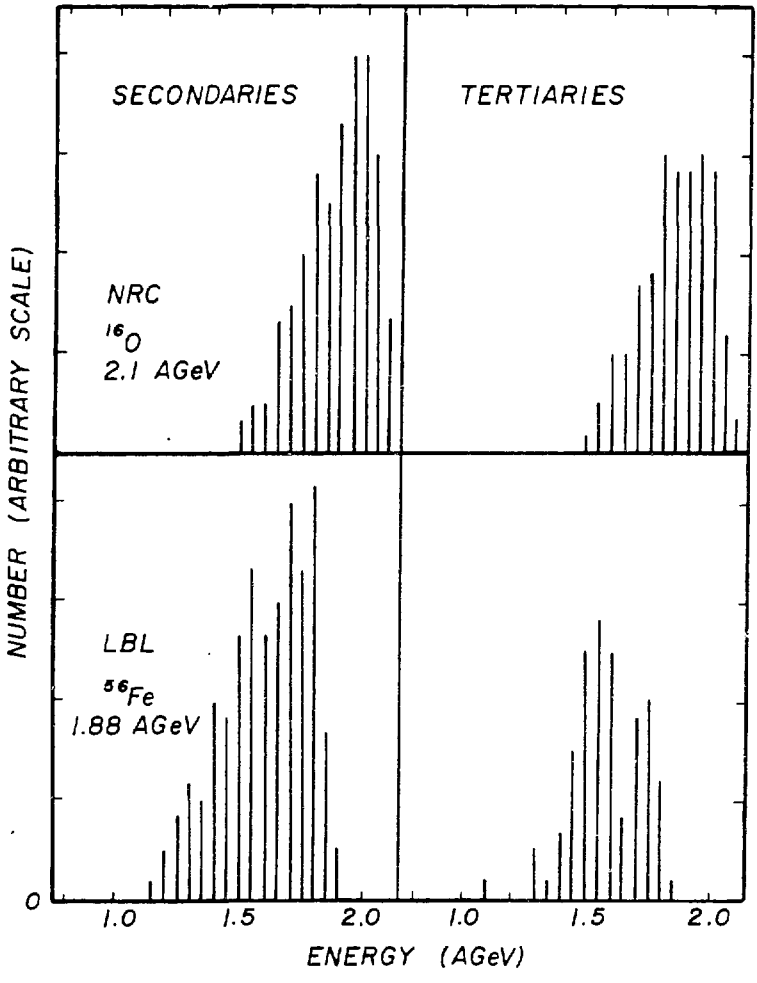

XBL 8110-7097

Fig. III-2a,b

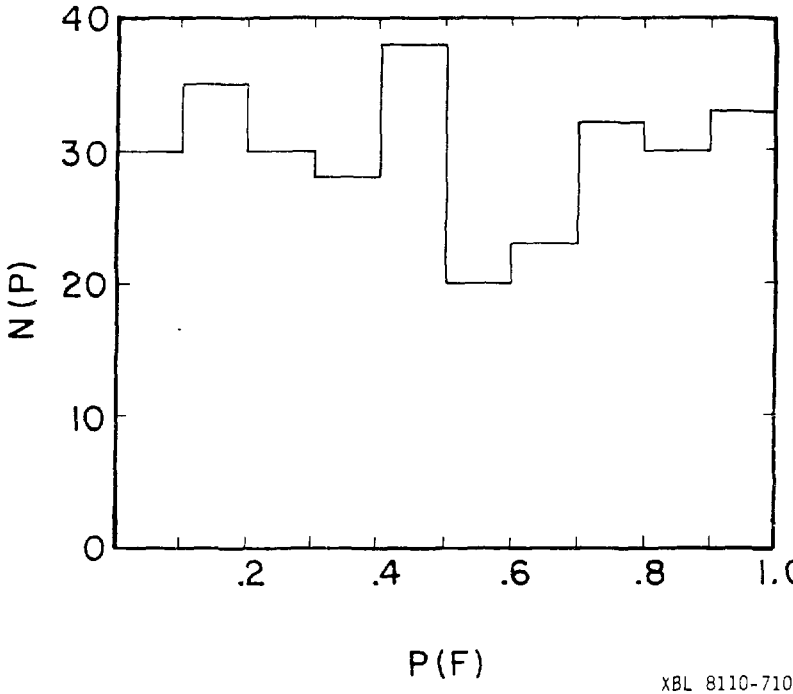

XBL 8110-7100

Fig. IV-1

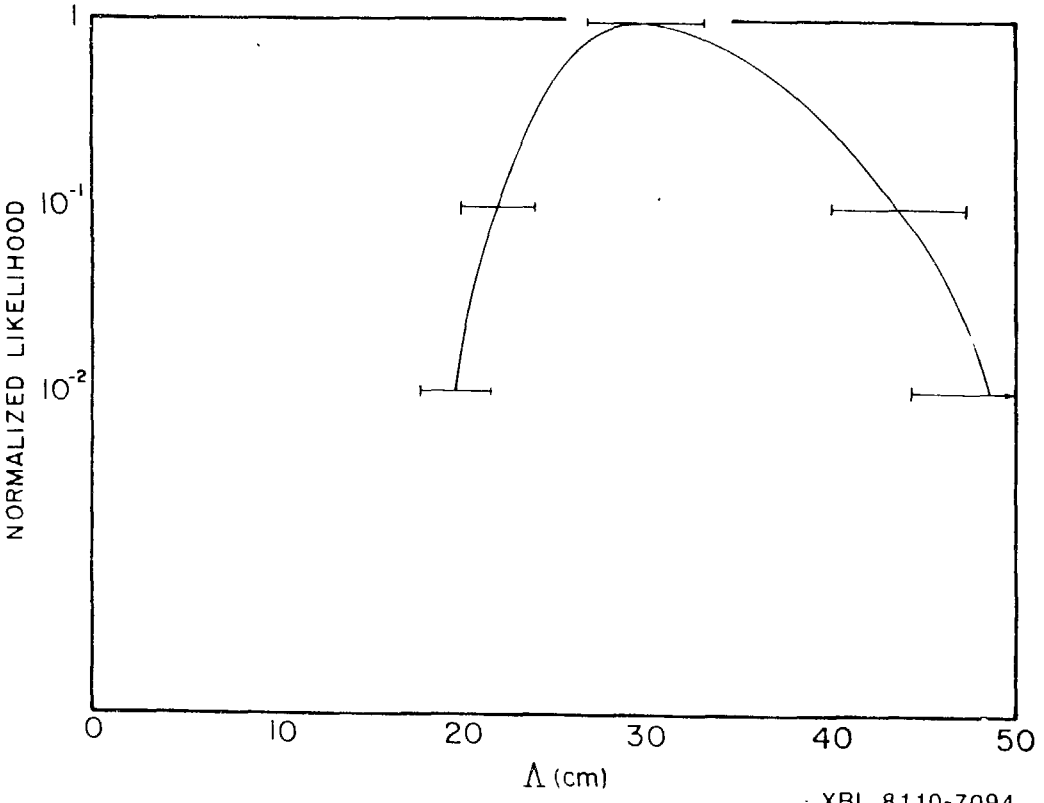

XBL 8110-7094

Fig. IV-2

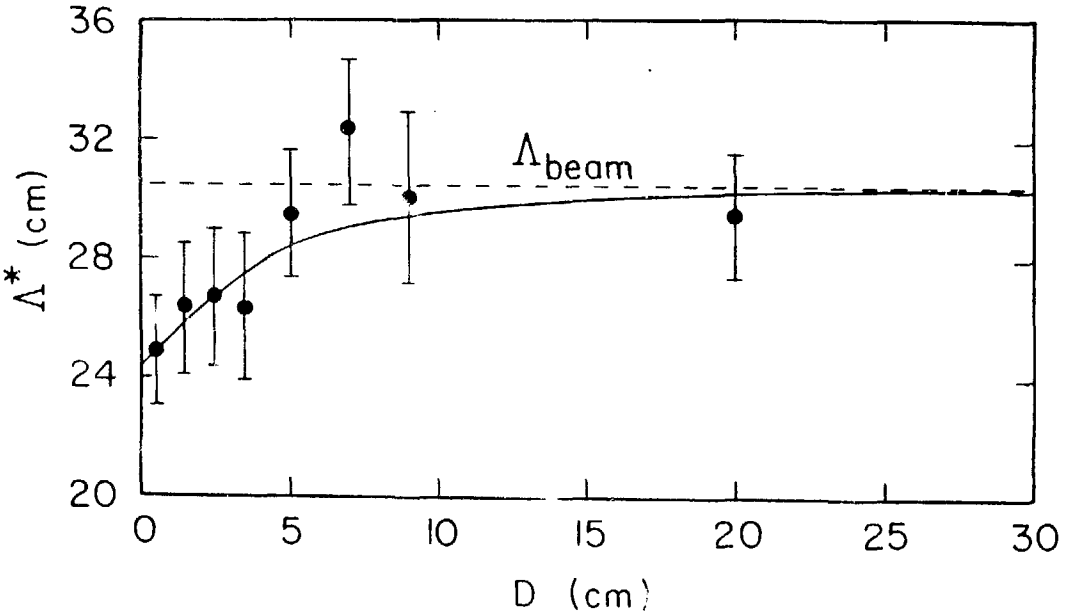

Fig. V-1

XBL 808-11485

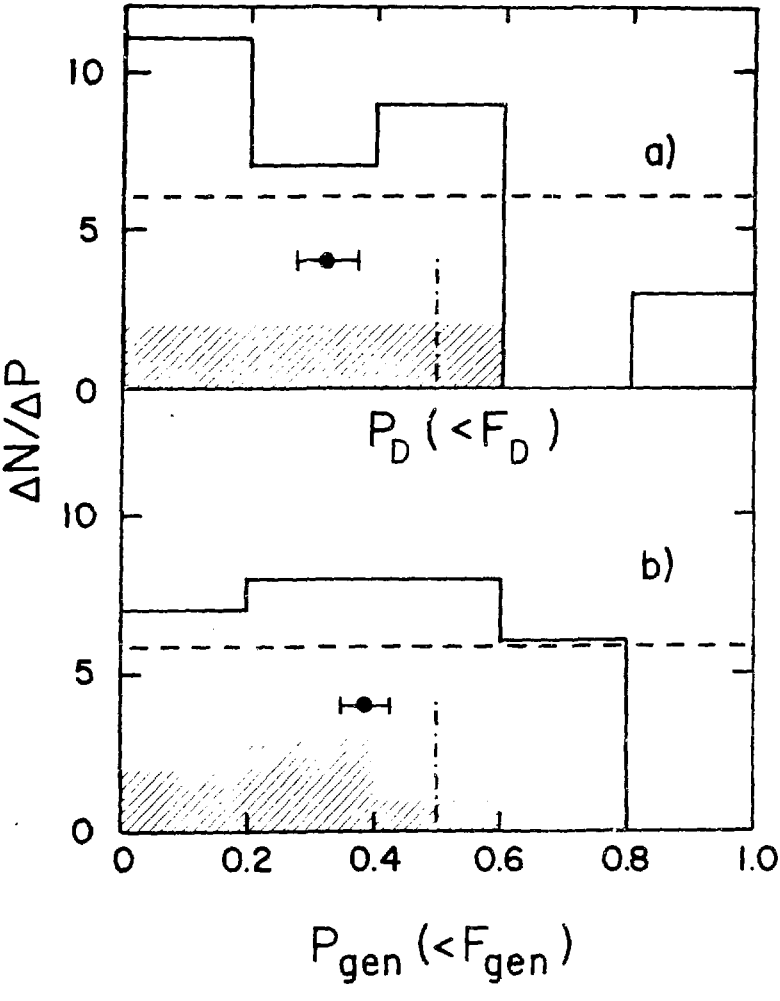

Fig. V-2

XBL 806-10260

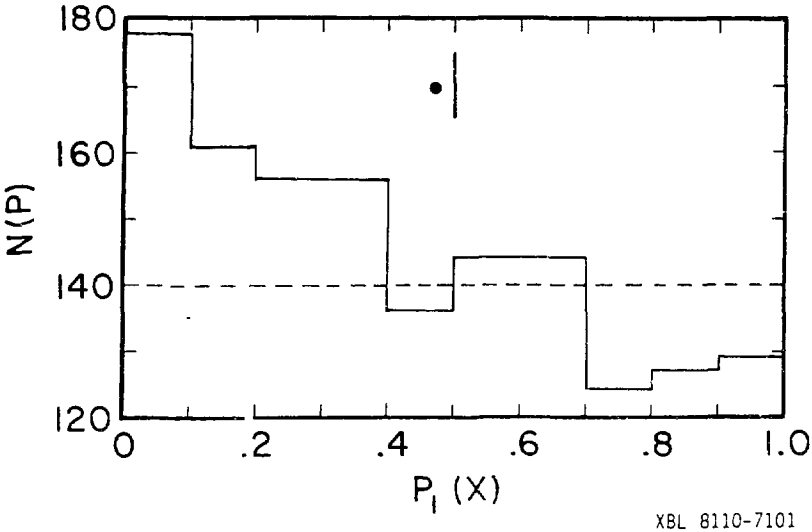

Fig. V-3

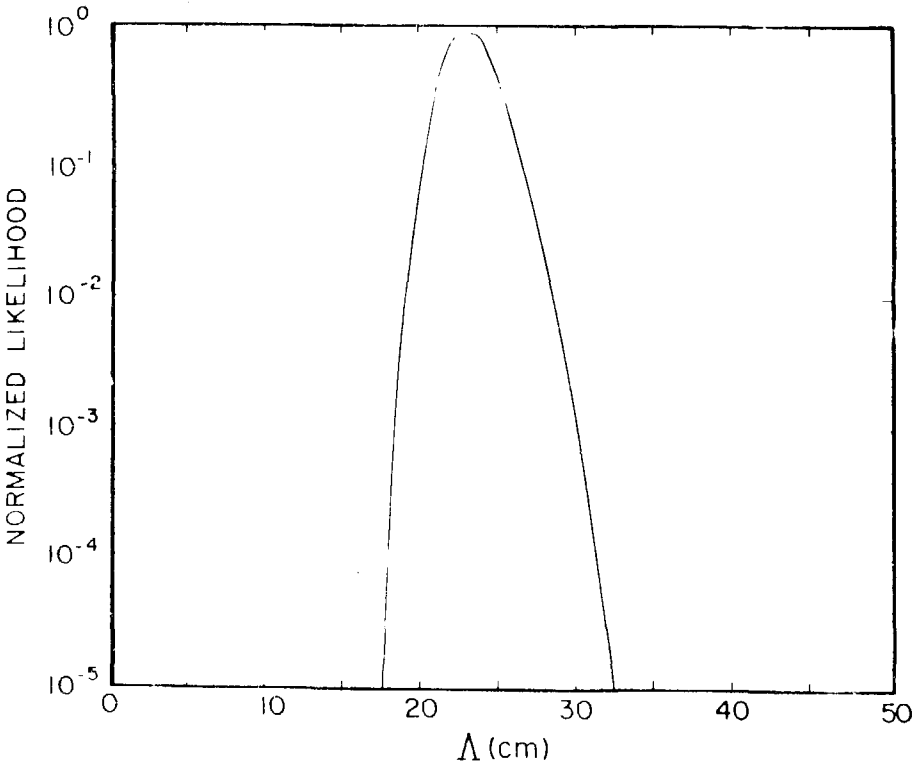

XBL 8110-7102

Fig. V-4

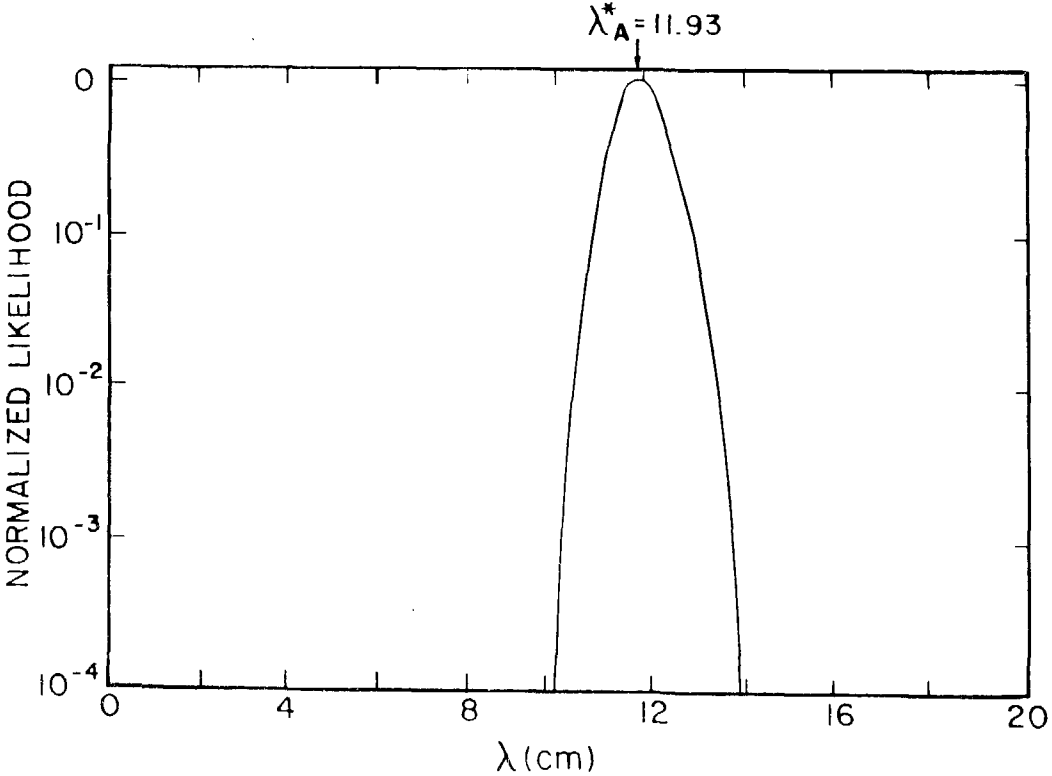

XBL 8110-7103

Fig. V-5

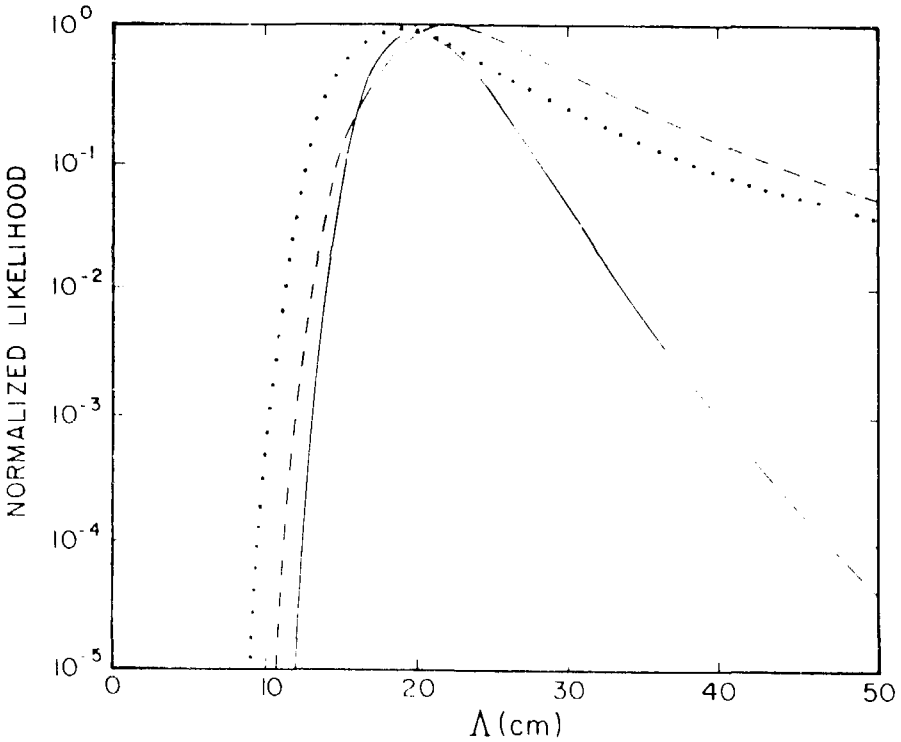

XBL 8110-7104

Fig. V.6

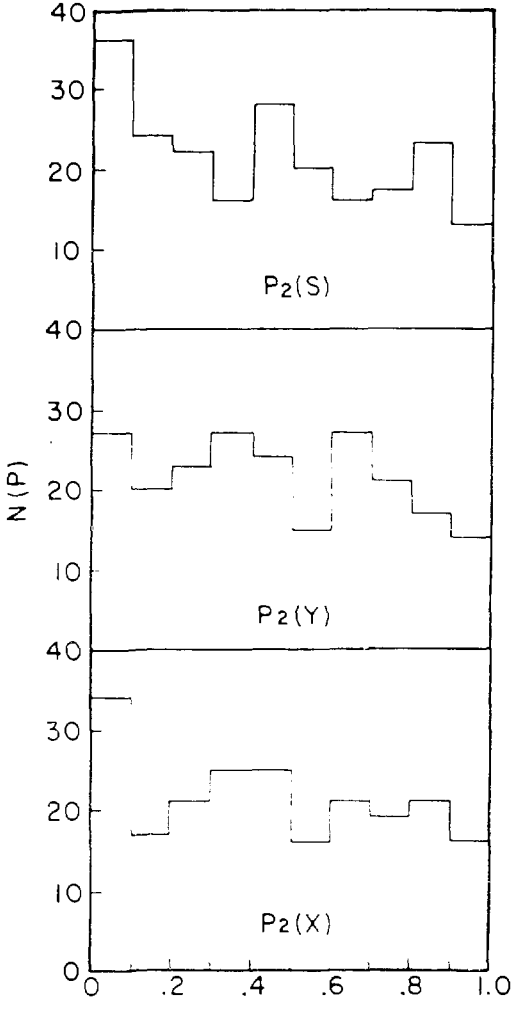

XBL 8110-1125

Fig. V-7

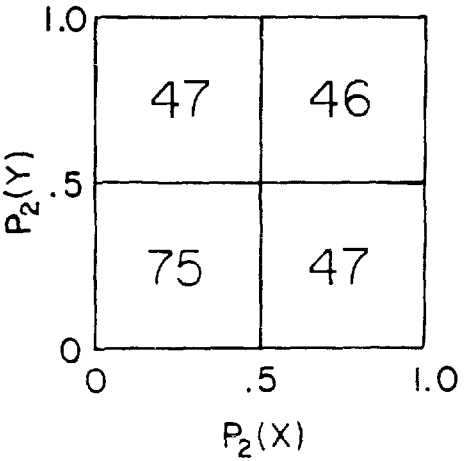

XBL 8110-7098

Fig. 4-8

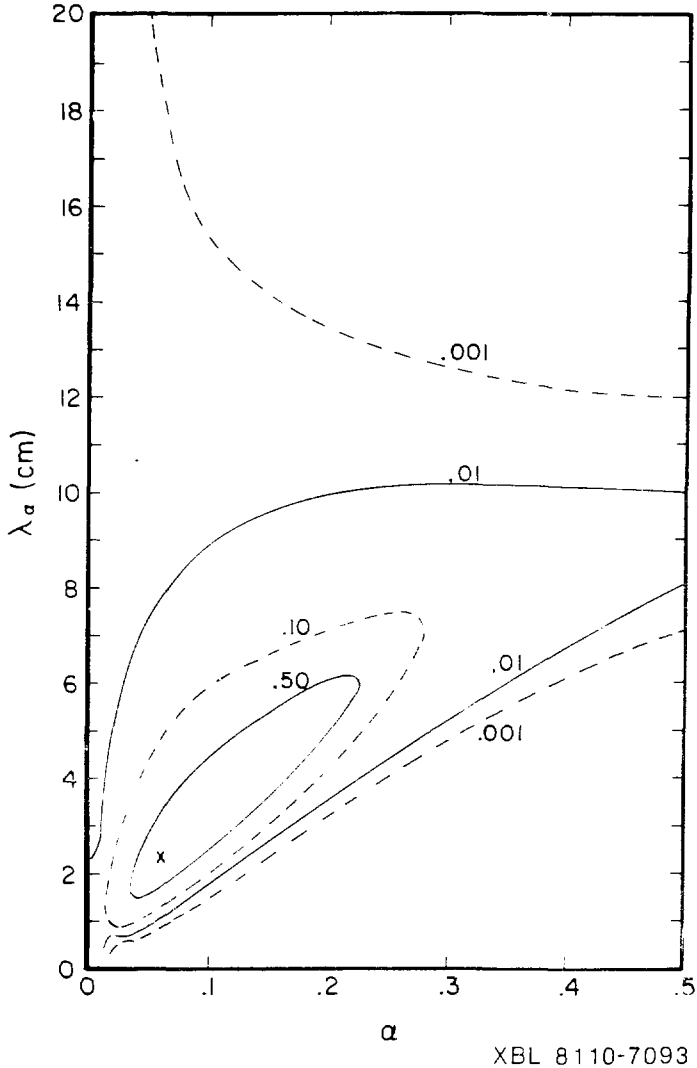

XBL 8110-7093

Fig. V-9

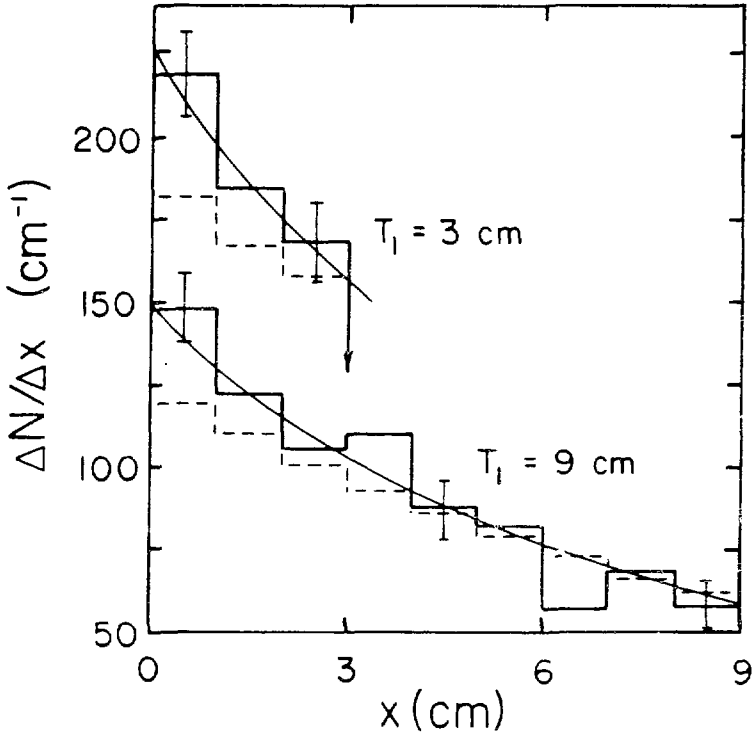

XBL 806-10262

Fig. V-10